International Journal of Engineering Science 230 (2027) 104697

Contents lists available at ScienceDirect

International Journal of Engineering Science

journal homepage: www.elsevier.com/locate/ijengsci

Full length article

Wave propagation and wrinkling localization in a prestressed periodic elastic half-space

Yuxin Fu [a], Michel Destrade [b], Yuesheng Wang [a], Yibin Fu [c,*]

[a] Department of Mechanics, Tianjin University, Tianjin 300072, China
[b] School of Mathematical and Statistical Sciences, University of Galway, Galway, Ireland
[c] School of Computing and Mathematics, Keele University, Staffordshire ST5 5BG, UK

ARTICLE INFO

Keywords:
Surface waves
Periodic half-space
Wrinkling
Bifurcation
Pattern formation
Nonlinear elasticity

ABSTRACT

We investigate surface waves in a prestressed elastic half-space whose material properties are constant in the vertical direction but vary periodically along the direction of wave propagation. Using Floquet-Bloch theory, Fourier expansion, and the Stroh formalism, we reduce the dynamic problem to the solution of a matrix Riccati equation for a high-dimensional (truncated) surface impedance matrix. Illustrative results are presented for the case in which each unit cell consists of two homogeneous materials. A two-term asymptotic expression for the wave speed is derived for wavenumbers near the edges of the Brillouin zone and is used to validate the numerical solutions. By increasing the prestress until the wave speed vanishes, we show that surface wrinkling in such a periodic half-space always localizes in the material that is more susceptible to instability and is not governed by homogenized properties. Furthermore, the critical prestress is found to be independent of the wavenumber, as in the classical homogeneous case, although surface waves remain dispersive before the onset of instability.

1. Introduction

Surface wave propagation is a fundamental problem in elastodynamics, with numerous practical applications. It also arises in a variety of related contexts, such as wave propagation in layered composites and coated half-spaces. Early studies primarily focused on homogeneous, unstressed elastic half-spaces. The existence and uniqueness of surface waves in a generally anisotropic elastic half-space was first settled by Barnett and Lothe (1974) with the aid of the Stroh formalism (Stroh, 1958, 1962), and then later formulated in terms of the surface impedance tensor by Barnett and Lothe (1985). Refinements were subsequently made by Chadwick and Smith (1977), Ting (1996), and further properties of the surface impedance tensor were established by Biryukov (1985), Fu and Mielke (2002) and Mielke and Fu (2004). We refer to the review article by Shuvalov (2024) for a summary of the latest developments.

With the surge of interest in metamaterials, attention naturally turned to surface waves in half-spaces with periodic material properties. Three types of periodic half-spaces may be distinguished: those that are periodic along the direction of wave propagation but homogeneous in depth (i.e. laterally periodic); those that are periodic in the depth direction but homogeneous along the direction of propagation; and those that are periodic in all directions, including half-spaces with periodic inclusions. Surface waves in half-spaces of the first type have previously been studied by Djafari-Rouhani et al. (1984) and Tanaka and Tamura (1998, 1999) by constructing solutions in terms of eigensolutions, by Norris et al. (2013) and Shuvalov (2024) using the Stroh formalism and matrix

* Corresponding author.
E-mail address: y.fu@keele.ac.uk (Y. Fu).

https://doi.org/10.1016/j.ijengsci.2026.104697
Received 27 August 2026; Received in revised form 24 September 2026; Accepted 24 September 2026
Available online 4 October 2026
0020-7225/© 2026 The Authors. Published by Elsevier Ltd. This is an open access article under the CC BY license (http://creativecommons.org/licenses/by/4.0/).

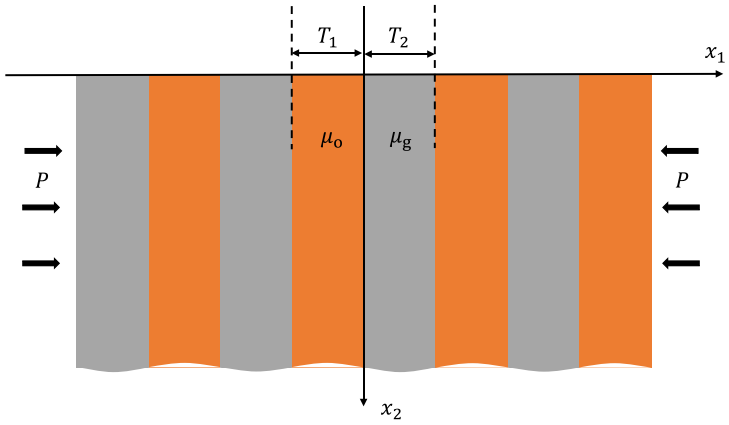


Fig. 1. Schematic of the periodic elastic half-space.

sign function method, by Hu et al. (2012) using the spectral method, by Matysiak et al. (2009) using a homogenized model with microlocal parameters, and by Pu and Shi (2017) using an energy method. Surface waves in half-spaces of the second type have been investigated by Shuvalov (2009) and by Darinskii and Shuvalov (2020) based on the Stroh formalism. Finally, for the case when the half-space is periodic in all directions, there exists a large body of literature based entirely on numerical calculations; see, e.g., Assouar and Oudich (2011), Khelif et al. (2010), Laude et al. (2005), Manzanares-Martinez and Ramos-Mendieta (2003), Tanaka et al. (2007), Wu et al. (2005, 2004), Yan and Wang (2008).

Another major extension of surface wave study is to prestressed elastic half-spaces for which the surface wave speed is a function of the prestress, so that a static surface wave mode becomes possible at a critical level of prestress. Surface wrinkling of a compressed homogeneous half-space was first studied by Green and Zerna (1954), Flavin (1963) and Biot (1963), who found that the critical stretch is approximately equal to 0.544 when the half-space is modeled as a neo-Hookean material and under plane strain prestress. This problem is nowadays commonly referred to as the Biot problem and the critical stretch as the Biot value. Subsequently, extensions were made to more general material models (Dowaikh & Ogden, 1990), general forms of prestress (Destrade & Ogden, 2005), and development of the Stroh formalism (Chadwick, 1997; Fu, 2005a, 2005b). It should be noted, however, that in reality surface wrinkling never occurs at the Biot value; in fact the problem of surface wrinkling is ill-posed in the sense that there does not exist a distinguished wavenumber and a post-buckling solution cannot be found by the usual near-critical post-bifurcation analysis (Ogden & Fu, 1996). Physically, it is localized creases rather than periodic surface wrinkles that have been observed (Gent & Cho, 1999), and similarly in Finite Element simulations (Hong et al., 2009). Mathematically, one can regularize the problem by adding a thin-layer/coating of a different material (Cai & Fu, 1999). On the other hand, surface wrinkling of a coated half-space (also commonly referred to as a film/substrate bilayer) itself has become a very active area of research, partly spurred on by the observation by Bowden et al. (1998) that the submicrometer patterns induced by surface wrinkling can serve a variety of useful purposes. We refer to Genzer and Groenewold (2006), Yang et al. (2010), Li et al. (2012), and Dimmock et al. (2020) for comprehensive reviews of the literature at various stages of the development.

Our current study is partially motivated by the observation that although recent studies have shown promise in using finite deformation and deformation-induced buckling to modulate wave propagation, see e.g. Wang and Bertoldi (2012), Rudykh and Boyce (2014), Li et al. (2016), and Li et al. (2018), these studies are mostly numerical and the fundamental problem of static surface wrinkling of a compressed periodic elastic half-space does not seem to have previously been studied although it is amenable to analysis. It is natural to approach this problem by starting from propagating surface waves in a pre-stressed periodic half-space and this is indeed the approach adopted in this paper.

We shall focus on the buckling behavior and wave characteristics of a periodic elastic half-space under compressive loading. As illustrated in Fig. 1, the periodic elastic half-space considered is piecewise homogeneous, but our methodology can be extended to more general variations in the x_1-direction. The orange and gray regions represent materials with different shear moduli (μ_o and μ_g, respectively) and both are assumed to have the same Poisson's ratio. The top surface of the structure is located at $x_2 = 0$ and is traction-free or subjected to a dead load. For fixed ν and equal densities, only two dimensionless parameters are involved in our analysis: the shear modulus ratio $\alpha = \mu_g/\mu_o$ and the width ratio $\delta = T_2/T$ where $T = T_1 + T_2$ is the cell length/period and T_2 the width of the gray material.

The rest of this paper is divided into five sections as follows. We start by formulating the problem and summarizing some necessary results concerning surface wave propagation in a homogeneous prestressed half-space that will be used in later sections. Then in Section 3, we combine the Floquet-Bloch theorem, Fourier expansion, and Stroh formulation to study surface waves in a pre-stressed elastic half-space, showing that after truncation the surface wave speed can be determined by setting the determinant of a surface impedance matrix to zero. Results are presented to show the dispersion relation in the first Brillouin zone and how it evolves as the pre-stress is increased. To verify our results, we carry out an asymptotic analysis in Section 4 for wave numbers close to either of the two end points of the Brillouin zone, following well-known methodologies given by e.g. Bensoussan et al. (1978),

Bakhvalov and Panasenko (1989), and Craster et al. (2010). A two-term asymptotic expression for the frequency is derived for each case and used to validate the results computed in Section 3. In Section 5, we turn our attention to static surface wrinkling and show that as a critical pre-stretch is approached, the frequency becomes zero independently of the wavenumber. A close examination of the bifurcation mode shows that the deformation always localize in the material that is more susceptible to surface wrinkling, and correspondingly the critical pre-stretch is determined by the Biot value for the corresponding material. In the final section, we summarize our results and make some additional comments.

2. Problem formulation

We first summarize the general incremental governing equations to be used in our later analysis. To this end, consider a general hyperelastic body B composed of a non-heat-conducting elastic material which possesses an initial unstressed state B_0. A purely homogeneous static deformation takes B_0 to a finitely stressed equilibrium configuration denoted by B_e. To study the dynamic and static properties of this finitely deformed configuration, we superimpose a small-amplitude displacement on B_e, and denote the resulting configuration by B_t. The position vectors of a representative particle are denoted by $\boldsymbol{X}$, $\boldsymbol{x}$ and $\tilde{\boldsymbol{x}}$ in B_0, B_e and B_t respectively, and we write

$$\tilde{\boldsymbol{x}} = \boldsymbol{x}(\boldsymbol{X}) + \boldsymbol{u}(\boldsymbol{x}, t), \tag{2.1}$$

where $\boldsymbol{u}$ is the incremental displacement associated with the deformation $B_e \to B_t$.

The deformation gradients arising from the deformations $B_0 \to B_e$ and $B_0 \to B_t$ and are denoted by $\bar{\boldsymbol{F}}$ and $\boldsymbol{F}$, respectively, and are defined by $d\boldsymbol{x} = \bar{\boldsymbol{F}} d\boldsymbol{X}$ and $d\tilde{\boldsymbol{x}} = \boldsymbol{F} d\boldsymbol{X}$. Thus, we have

$$\boldsymbol{F} = (\boldsymbol{I} + \operatorname{grad} \boldsymbol{u})\bar{\boldsymbol{F}}, \qquad F_{iA} = (\delta_{ij} + u_{i,j})\bar{F}_{jA}, \tag{2.2}$$

where $\boldsymbol{I}$ is the identity tensor, $\operatorname{grad} \boldsymbol{u}$ denotes the gradient of $\boldsymbol{u}$ with respect to $\boldsymbol{x}$, and here and henceforth a comma indicates differentiation with respect to the implied rectangular coordinate of $\boldsymbol{x}$. Furthermore, the convention whereby upper case indices refer to coordinates in B_0 and lower case indices to coordinates in B_e will be observed.

The constitutive equation is given by

$$\boldsymbol{S} = \frac{\partial W}{\partial \boldsymbol{F}}, \qquad S_{Ai} = \frac{\partial W}{\partial F_{iA}}, \tag{2.3}$$

where $\boldsymbol{S}$ is the nominal stress and W is the strain–energy function, assumed to be a function of $\boldsymbol{F}$ and measured per unit volume in the reference configuration.

It is convenient to define an incremental stress tensor χ through

$$\chi = \bar{J}^{-1}(\tilde{\boldsymbol{S}}^T - \bar{\boldsymbol{S}}^T)\bar{\boldsymbol{F}}^T, \tag{2.4}$$

where $\bar{J} = \det \bar{\boldsymbol{F}}$, and $\bar{\boldsymbol{S}}$ and $\tilde{\boldsymbol{S}}$ are the nominal stresses in B_{e} and B_t, respectively. It can then be shown that χ satisfies the equation of motion

$$\operatorname{div} \chi^T = \rho \ddot{\boldsymbol{u}}, \qquad \chi_{ij,j} = \rho \ddot{u}_i, \tag{2.5}$$

where ρ is the material density in B_e. Linearizing the right hand side of (2.4), we obtain

$$\chi_{ij} = \mathcal{A}_{jilk} u_{k,l}, \tag{2.6}$$

where $\mathcal{A}_{jilk}$ are the first-order instantaneous elastic moduli in B_{e} that are defined by (Chadwick & Ogden, 1971)

$$\mathcal{A}_{jilk} = \bar{J}^{-1} \bar{F}_{jA} \bar{F}_{lB} \left. \frac{\partial^2 W}{\partial F_{iA} \partial F_{kB}} \right|_{\boldsymbol{F}=\bar{\boldsymbol{F}}}. \tag{2.7}$$

In terms of the principal stretches, the non-zero components of $\boldsymbol{\mathcal{A}}$ in the orthonormal basis aligned with the principal directions of strain can be computed according to the following formulae:

$$\begin{aligned} &\bar{J}\mathcal{A}_{iijj} = \lambda_i \lambda_j W_{ij}, \\ &\bar{J}\mathcal{A}_{ijkl} = \frac{\lambda_i^2}{\lambda_i^2 - \lambda_j^2}(\lambda_i W_i - \lambda_j W_j)\delta_{ik}\delta_{jl} + \frac{\lambda_i \lambda_j}{\lambda_i^2 - \lambda_j^2}(\lambda_j W_i - \lambda_i W_j)\delta_{il}\delta_{jk}, \qquad i \neq j, \end{aligned} \tag{2.8}$$

where $W_i = \partial W / \partial \lambda_i$, $W_{ij} = \partial^2 W / \partial \lambda_i \partial \lambda_j$, and the principal stretches are understood to correspond to the primary deformation $B_0 \to B_e$.

For our illustrative calculations, we assume that the strain energy function for both materials is given by

$$W = \frac{\mu}{2}\left(I_1 - 3 - 2\log J\right) + \frac{\mu\nu}{1-2\nu}(J-1)^2, \tag{2.9}$$

where μ and ν are the ground-state shear modulus and Poisson's ratio, respectively, I_1 is the first invariant of the right Cauchy–Green tensor, and J is the determinant of the deformation gradient $\boldsymbol{F}$. We assume that the two materials have the same Poisson ratio which we take to be 0.4999 (almost incompressible) in all of our illustrative calculations unless otherwise stated. As indicated earlier, the shear moduli are denoted by μ_{g} and μ_{o} and are generally different.

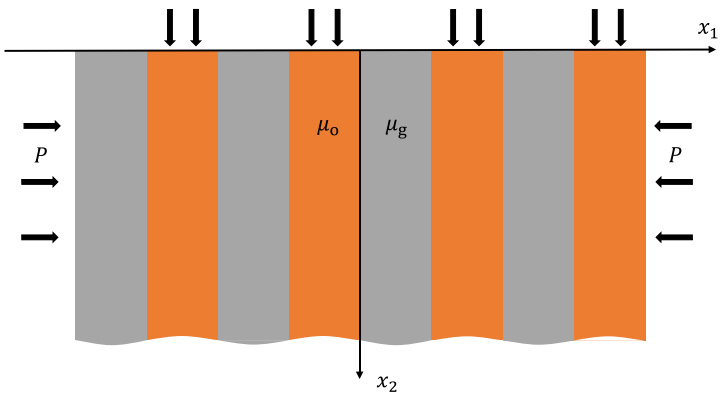


Fig. 2. Schematic of the actual periodic elastic half-space studied.

We now specialize the above governing equations to a laterally periodic hyperelastic half-space that is subjected to a plane strain compression in the x_1-direction; see Fig. 2. Because the resulting deformation will generally be nonhomogeneous, to make analysis possible, we assume that the softer material, signified by the orange color, is also subjected to a compression in the vertical direction such that the resulting deformation is piecewise homogeneous in the periodic half-space. Thus, we may assume that the deformation gradients in the orange and gray materials are given by

$$\bar{\boldsymbol{F}}^{\mathrm{o}} = \lambda_1^{\mathrm{o}} \boldsymbol{e}_1 \otimes \boldsymbol{E}_1 + \lambda_2 \boldsymbol{e}_2 \otimes \boldsymbol{E}_2, \qquad \bar{\boldsymbol{F}}^{\mathrm{g}} = \lambda_1^{\mathrm{g}} \boldsymbol{e}_1 \otimes \boldsymbol{E}_1 + \lambda_2 \boldsymbol{e}_2 \otimes \boldsymbol{E}_2, \tag{2.10}$$

respectively, where we have made use of the fact that λ_2 is the same for both materials due to displacement continuity, and used superscripts g and o to signify association with the gray and orange materials, respectively. The overall stretch λ_1 in the x_1-direction is then given by

$$\lambda_1 = \lambda_1^{\mathrm{o}}(1-\delta) + \lambda_1^{\mathrm{g}}\delta. \tag{2.11}$$

Given a λ_1^{g}, we solve $\bar{S}_{22}^{\mathrm{g}} = 0$ to find λ_2, then solve the traction continuity condition $\bar{S}_{11}^{\mathrm{g}} = \bar{S}_{11}^{\mathrm{o}}$ to find λ_1^{o}, and finally use (2.11) to compute the overall stretch λ_1. Conversely, when λ_1 is specified, the stretches λ_2, λ_1^{o} and λ_1^{g} can be determined by solving three nonlinear algebraic equations. Once λ_1^{o} and λ_2 are known, the $\bar{S}_{22}^{\mathrm{o}}$ in the orange/soft material will in general be non-zero, which is the surface traction required to maintain the homogeneous deformation (2.10) in the entire half-space.

3. Propagation of surface waves

Assuming harmonic motion with angular frequency ω, the governing equations and boundary conditions reduce to

$$\chi_{ij,j} = \left(\mathcal{A}_{jilk}(x_1)u_{k,l}\right)_{,j} = -\omega^2 \rho(x_1) u_i, \tag{3.1}$$

$$t_i \equiv \chi_{i2} = \mathcal{A}_{2ilk}(x_1)u_{k,l} = 0, \qquad x_2 = 0, \tag{3.2}$$

where $\mathcal{A}_{jilk}$ and ρ are both T-periodic. The solution should also satisfy the decaying condition $u_k \to 0$ as $x_2 \to \infty$, but this condition is not displayed explicitly here and hereafter.

These equations can be rewritten as

$$\left\{\boldsymbol{Q}(x_1)\boldsymbol{u}_{,1} + \boldsymbol{R}(x_1)\boldsymbol{u}_{,2}\right\}_{,1} + \boldsymbol{t}_{,2} = -\omega^2 \boldsymbol{\rho}(x_1)\boldsymbol{u}, \tag{3.3a}$$

$$\boldsymbol{t} \equiv \boldsymbol{R}^T(x_1)\boldsymbol{u}_{,1} + \boldsymbol{T}(x_1)\boldsymbol{u}_{,2} = \boldsymbol{0}, \qquad x_2 = 0, \tag{3.3b}$$

where $\boldsymbol{\rho}(x_1) = \rho(x_1)\boldsymbol{I}$, and the matrix functions $\boldsymbol{Q}(x_1)$, $\boldsymbol{R}(x_1)$, and $\boldsymbol{T}(x_1)$ are defined by their components

$$Q_{ik}(x_1) = \mathcal{A}_{1i1k}(x_1), \qquad R_{ik}(x_1) = \mathcal{A}_{1i2k}(x_1), \qquad T_{ik}(x_1) = \mathcal{A}_{2i2k}(x_1). \tag{3.4}$$

3.1. Homogeneous half-space

We first summarize some well-known results for the special case when the half-space is homogeneous so that the elastic moduli $\mathcal{A}_{jilk}$ and density ρ are all constants. In this case, if we look for a surface wave solution of the form

$$\boldsymbol{u} = \boldsymbol{z}(kx_2)\mathrm{e}^{\mathrm{i}kx_1}, \qquad \boldsymbol{t} = k\boldsymbol{w}(kx_2)\mathrm{e}^{\mathrm{i}kx_1}, \tag{3.5}$$

where k is a positive constant, then Eqs. (3.3a) and (3.3b) reduce to

$$\boldsymbol{T}\boldsymbol{z}'' + \mathrm{i}(\boldsymbol{R} + \boldsymbol{R}^T)\boldsymbol{z}' - \boldsymbol{Q}_v\boldsymbol{z} = \boldsymbol{0}, \tag{3.6a}$$

$$\boldsymbol{w} = \mathrm{i}\boldsymbol{R}^T\boldsymbol{z} + \boldsymbol{T}\boldsymbol{z}' = \boldsymbol{0}, \qquad x_2 = 0, \tag{3.6b}$$

where $\boldsymbol{Q}_v = \boldsymbol{Q} - \rho v^2\boldsymbol{I}$ and $v = \omega/k$. These two equations may be re-arranged into the form

$$\boldsymbol{z}' = \boldsymbol{T}^{-1}\boldsymbol{w} - \mathrm{i}\boldsymbol{T}^{-1}\boldsymbol{R}^T\boldsymbol{z}, \tag{3.7a}$$

$$\boldsymbol{w}' = (\boldsymbol{Q}_v - \boldsymbol{R}\boldsymbol{T}^{-1}\boldsymbol{R}^T)\boldsymbol{z} - \mathrm{i}\boldsymbol{R}\boldsymbol{T}^{-1}\boldsymbol{w}, \tag{3.7b}$$

or equivalently the Stroh/Hamiltonian form

$$\frac{\mathrm{d}}{\mathrm{d}x_2}\begin{pmatrix}\boldsymbol{z}\\ \boldsymbol{w}\end{pmatrix} = \begin{pmatrix}-\mathrm{i}\boldsymbol{T}^{-1}\boldsymbol{R}^T & \boldsymbol{T}^{-1}\\ \boldsymbol{Q}_v - \boldsymbol{R}\boldsymbol{T}^{-1}\boldsymbol{R}^T & -\mathrm{i}\boldsymbol{R}\boldsymbol{T}^{-1}\end{pmatrix}\begin{pmatrix}\boldsymbol{z}\\ \boldsymbol{w}\end{pmatrix}. \tag{3.8}$$

The problem can then be solved by introducing the surface impedance matrix $\boldsymbol{M}$ through

$$\boldsymbol{w}(0) = -\boldsymbol{M}\boldsymbol{z}(0), \tag{3.9}$$

which also implies that

$$\boldsymbol{w}(y) = -\boldsymbol{M}\boldsymbol{z}(y) \qquad \forall\ y \equiv kx_2 > 0 \tag{3.10}$$

since the material is homogeneous in the x_2-direction (depth direction) and so the relationship between $\boldsymbol{w}$ and $\boldsymbol{z}$ should be independent of x_2. The minus sign in (3.9) is due to the fact that the actual traction is minus $\boldsymbol{w}(0)$ since the outward normal to the surface is $-\boldsymbol{e}_2$.

Substituting Eq. (3.10) into (3.8), eliminating $\boldsymbol{z}$ and noting that the resulting equation is valid for arbitrary $\boldsymbol{z}$, we obtain the Riccati equation (Biryukov, 1985; Fu & Mielke, 2002)

$$(\boldsymbol{M} - \mathrm{i}\boldsymbol{R})\boldsymbol{T}^{-1}(\boldsymbol{M} + \mathrm{i}\boldsymbol{R}^T) - \boldsymbol{Q}_v = \boldsymbol{0}. \tag{3.11}$$

The traction-free boundary condition is obviously given by $\boldsymbol{M}\boldsymbol{z}(0) = \boldsymbol{0}$. Thus, the surface wave speed v is determined by

$$\det(\boldsymbol{M}) = 0. \tag{3.12}$$

It is now well-known that in the subsonic interval, $\boldsymbol{M}$ is Hermitian so that (3.12) is always a real expression, and that its real eigenvalues are monotonic functions of v so that the unique root of (3.12) can be determined in a robust manner.

To compute $\boldsymbol{z}(y)$, we substitute the trial solution

$$\boldsymbol{z}(y) = \mathrm{e}^{-\boldsymbol{E}y}\boldsymbol{z}(0) \tag{3.13}$$

and (3.10) into (3.7a) to obtain

$$\boldsymbol{E} = \boldsymbol{T}^{-1}(\boldsymbol{M} + \mathrm{i}\boldsymbol{R}^T). \tag{3.14}$$

It was shown in Fu and Mielke (2002) that the Riccati equation (3.11) subject to (3.12) has a unique positive definite or positive semi-definite solution for $\boldsymbol{M}$, and that the corresponding $\boldsymbol{E}$ computed from (3.14) has the property that all its eigenvalues have positive real parts so that $\boldsymbol{z}(x_2)$ given by (3.13) decays exponentially as $x_2 \to \infty$.

Setting $v = 0$ and viewing $\det(\boldsymbol{M})$ as a function of the pre-stretch, Eq. (3.12) then becomes a bifurcation condition that can be solved to find the Biot value, the critical stretch for surface wrinkling.

3.2. Periodic half-space

According to the Floquet-Bloch theory, the displacement $\boldsymbol{u}$ and traction vector $\boldsymbol{t}$ can each be represented as $\mathrm{e}^{\mathrm{i}kx_1}$ times a T-periodic vector function. Since each T-periodic function can be represented by a Fourier series, we have

$$\boldsymbol{u} = e^{\mathrm{i}kx_1}\sum_{n=-\infty}^{+\infty}\boldsymbol{z}_n(x_2)\mathrm{e}^{\mathrm{i}g_nx_1} = \sum_{n=-\infty}^{+\infty}\boldsymbol{z}_n(x_2)\mathrm{e}^{\mathrm{i}k_nx_1}, \tag{3.15a}$$

$$\boldsymbol{t} = \mathrm{e}^{\mathrm{i}kx_1}\sum_{n=-\infty}^{+\infty}\boldsymbol{w}_n(x_2)\mathrm{e}^{\mathrm{i}g_nx_1} = \sum_{n=-\infty}^{+\infty}\boldsymbol{w}_n(x_2)\mathrm{e}^{\mathrm{i}k_nx_1}, \tag{3.15b}$$

where $k_n = k + g_n$ and $g_n = 2n\pi/T$. We also represent the T-periodic matrix functions $\boldsymbol{Q}(x_1)$, $\boldsymbol{R}(x_1)$, $\boldsymbol{T}(x_1)$ and $\boldsymbol{\rho}(x_1)$ by their Fourier series:

$$\{\boldsymbol{Q}(x_1), \boldsymbol{R}(x_1), \boldsymbol{T}(x_1), \boldsymbol{\rho}(x_1)\} = \sum_{n=-\infty}^{+\infty}\{\boldsymbol{Q}^{(n)}, \boldsymbol{R}^{(n)}, \boldsymbol{T}^{(n)}, \boldsymbol{\rho}^{(n)}\}\ \mathrm{e}^{\mathrm{i}g_nx_1}. \tag{3.16}$$

It then follows, e.g., that

$$\begin{aligned}(\boldsymbol{Q}(x_1)\boldsymbol{u}_{,1})_{,1} &= \frac{\partial}{\partial x_1}\left(\sum_{n=-\infty}^{+\infty}\left(\boldsymbol{Q}^{(n)}\mathrm{e}^{\mathrm{i}g_nx_1}\right)\sum_{n=-\infty}^{+\infty}\left(\mathrm{i}k_n\boldsymbol{z}_n(x_2)\mathrm{e}^{\mathrm{i}k_nx_1}\right)\right)\\ &= -\sum_{n=-\infty}^{+\infty}\sum_{m=-\infty}^{+\infty}\left(k_nk_m\boldsymbol{Q}^{(n-m)}\boldsymbol{z}_m(x_2)\right)\ \mathrm{e}^{\mathrm{i}k_nx_1}.\end{aligned} \tag{3.17}$$

Similar expressions may be written down for the other terms in (3.3a) and (3.3b). On equating the coefficients of $e^{ik_n x_1}$ in (3.3a) and (3.3b), and truncating the infinite sums, we obtain

$$\boldsymbol{w}_n'(x_2) = \sum_{m=-N}^{+N} \left(k_n k_m \boldsymbol{Q}^{(n-m)} \boldsymbol{z}_m(x_2) - \omega^2 \boldsymbol{\rho}^{(n-m)} \boldsymbol{z}_m(x_2) - \mathrm{i} k_n \boldsymbol{R}^{(n-m)} \boldsymbol{z}_m'(x_2) \right), \tag{3.18}$$

$$\boldsymbol{w}_n(x_2) = \sum_{m=-N}^{+N} \left(\mathrm{i} k_m \boldsymbol{R}^{T(n-m)} \boldsymbol{z}_m(x_2) + \boldsymbol{T}^{(n-m)} \boldsymbol{z}_m'(x_2) \right), \tag{3.19}$$

where $n = 0, \pm 1, \pm 2, \ldots \pm N$, and N is a suitably large positive integer.

Following Norris et al. (2013) and Shuvalov (2024), we may rewrite these equations in an augmented matrix form in terms of the notations

$$\boldsymbol{w}(x_2) = \begin{pmatrix} \boldsymbol{w}_{-N} \\ \vdots \\ \boldsymbol{w}_0 \\ \vdots \\ \boldsymbol{w}_N \end{pmatrix}, \qquad \boldsymbol{z}(x_2) = \begin{pmatrix} \boldsymbol{z}_{-N} \\ \vdots \\ \boldsymbol{z}_0 \\ \vdots \\ \boldsymbol{z}_N \end{pmatrix},$$

and

$$\widetilde{\boldsymbol{Q}}_{(n,m)} = k_n k_m \boldsymbol{Q}^{(n-m)}, \qquad \widetilde{\boldsymbol{R}}_{(n,m)} = k_n \boldsymbol{R}^{(n-m)}, \qquad \widetilde{\boldsymbol{T}}_{(n,m)} = \boldsymbol{T}^{(n-m)}, \qquad \widetilde{\boldsymbol{\rho}}_{(n,m)} = \boldsymbol{\rho}^{(n-m)}.$$

The result is

$$\boldsymbol{w}(x_2) = \mathrm{i} \widetilde{\boldsymbol{R}}^H \boldsymbol{z}(x_2) + \widetilde{\boldsymbol{T}} \boldsymbol{z}'(x_2), \tag{3.20a}$$

$$\boldsymbol{w}'(x_2) = \left(\widetilde{\boldsymbol{Q}} - \omega^2 \widetilde{\boldsymbol{\rho}} \right) \boldsymbol{z}(x_2) - \mathrm{i} \widetilde{\boldsymbol{R}} \boldsymbol{z}'(x_2), \tag{3.20b}$$

where the superscript H signifies Hermitian conjugation (i.e. conjugate transpose) and the $2(2N+1) \times 2(2N+1)$ matrices $\widetilde{\boldsymbol{Q}}$, $\widetilde{\boldsymbol{R}}$, $\widetilde{\boldsymbol{T}}$, and $\widetilde{\boldsymbol{\rho}}$ are partitioned in terms of 2×2 matrices, with their (n,m)-th block given by

$$\widetilde{\boldsymbol{Q}}_{(n,m)}, \qquad \widetilde{\boldsymbol{R}}_{(n,m)}, \qquad \widetilde{\boldsymbol{T}}_{(n,m)}, \qquad \widetilde{\boldsymbol{\rho}}_{(n,m)},$$

respectively, where $m, n = -N, \ldots, 0, \ldots, N$.

By defining $\widetilde{\boldsymbol{Q}}_d = \widetilde{\boldsymbol{Q}} - \omega^2 \widetilde{\boldsymbol{\rho}}$ and rearranging, Eqs. (3.20b) and (3.20a) can be rewritten as (Norris et al., 2013)

$$\frac{\mathrm{d}}{\mathrm{d}x_2} \begin{pmatrix} \boldsymbol{z} \\ \boldsymbol{w} \end{pmatrix} = \begin{pmatrix} -\mathrm{i} \widetilde{\boldsymbol{T}}^{-1} \widetilde{\boldsymbol{R}}^H & \widetilde{\boldsymbol{T}}^{-1} \\ \widetilde{\boldsymbol{Q}}_d - \widetilde{\boldsymbol{R}} \widetilde{\boldsymbol{T}}^{-1} \widetilde{\boldsymbol{R}}^H & -\mathrm{i} \widetilde{\boldsymbol{R}} \widetilde{\boldsymbol{T}}^{-1} \end{pmatrix} \begin{pmatrix} \boldsymbol{z} \\ \boldsymbol{w} \end{pmatrix}. \tag{3.21}$$

Then the rest of the analysis is similar to that for a homogeneous half-space. The surface impedance matrix $\boldsymbol{M}$ is defined by

$$\boldsymbol{w}(0) = -\boldsymbol{M} \boldsymbol{z}(0), \tag{3.22}$$

and satisfies the Riccati equation

$$(\boldsymbol{M} - \mathrm{i} \widetilde{\boldsymbol{R}}) \widetilde{\boldsymbol{T}}^{-1} (\boldsymbol{M} + \mathrm{i} \widetilde{\boldsymbol{R}}^H) - \widetilde{\boldsymbol{Q}_d} = \boldsymbol{0}, \tag{3.23}$$

and the dispersion relation

$$\det(\boldsymbol{M}) = 0. \tag{3.24}$$

The above augmented surface impedance matrix enjoys almost all of the properties that its counterpart for a homogeneous half-space has, although it is now dependent on the wavenumber k (Shuvalov, 2024). Better still, the symbolic manipulation package *Mathematica* has a dedicated command **RiccatiSolve** that can be used to find the unique solution of (3.23) and (3.24) that is positive semi-definite in the subsonic interval.

The dispersion relation (3.24) defines the angular frequency ω as an implicit function of the wavenumber k. We first consider prestresses such that the surface impedance matrix $\boldsymbol{M}$ is positive definite when $\omega = 0$. For each fixed k, we find the associated ω by increasing ω from zero until (3.24) is satisfied. Instead of computing $\det(\boldsymbol{M})$, which may become extremely large, we replace (3.24) by the condition that the smallest eigenvalue of $\boldsymbol{M}$ vanishes.

Results are displayed in terms of the non-dimensional frequency ω_s and wave speed v_s defined by

$$\omega_s = \omega T / v_\mathrm{o}, \qquad v_s = v / v_\mathrm{o}, \qquad \text{where } v_\mathrm{o} = \sqrt{\mu_\mathrm{o} / \rho_\mathrm{o}}. \tag{3.25}$$

A convergence test was first conducted for the case when there is no prestress ($\lambda_1 = 1$). Fig. 3(a) displays the analytical results with truncation numbers $N = 3, 10, 15$ against the corresponding numerical results obtained using the Finite Element software *Abaqus* (Aberg & Gudmundson, 1997). It is seen that even for N as small as 3, the results are graphically indistinguishable from the *Abaqus* simulation results. Nonetheless, as Fig. 3(b) shows, when zoomed in, some minor differences can still be detected. For instance, at $kT = \pi$, the frequencies corresponding to $N = 3$ and 15 are 3.25397 and 3.23964, respectively, which approximate the *Abaqus* result

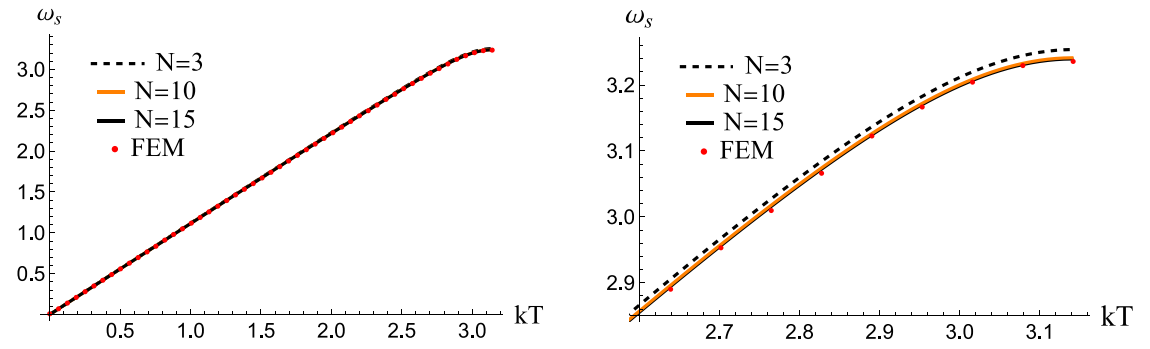


Fig. 3. Comparison between analytical results with different truncation numbers and the Abaqus simulation results with $\alpha = 2$, $\delta = 0.5$, $\rho_o = \rho_g = 1$. The right figure is a zoomed-in version of left figure, showing the minor differences between the four sets of results.

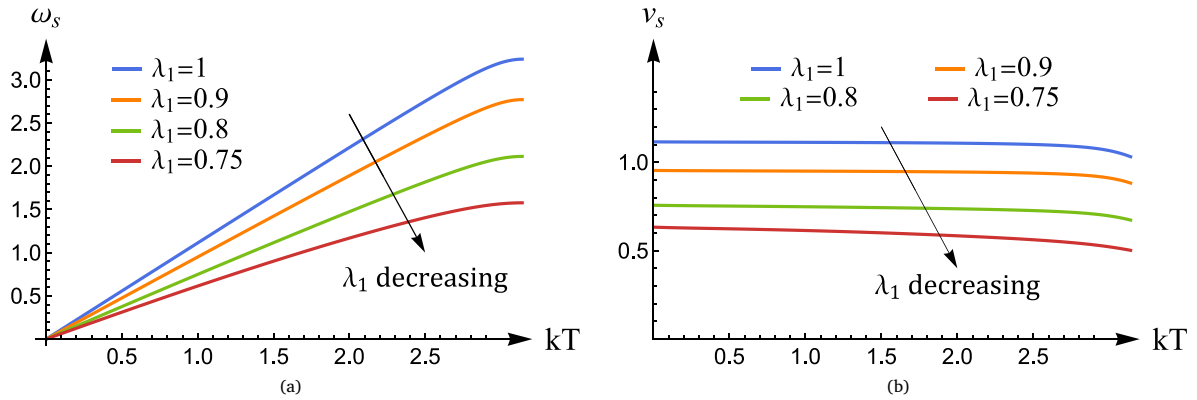


Fig. 4. Dispersion relations for the nondimensional (a) frequency and (b) wave speed under increasing compressive strains (as indicated by the arrows) when $\alpha = 2$ and $\delta = 0.5$.

of 3.23584 with a relative error less than 0.6% and 0.2%, respectively. Based on this observation and the fact that each calculation takes only a few seconds on a typical desktop, we conservatively take $N = 15$ in all of our subsequent calculations.

For a typical parameter set with $\alpha = 2$ (stiffness ratio), $\delta = 0.5$ (length ratio), and $\rho_o = \rho_g = 1$, the dependence of ω_s and v_s on kT is presented in Fig. 4 for different stretch ratios. Profiles of ω_s and v_s are symmetric about $kT = \pi$ over the Brillouin zone $[0, 2\pi]$, so they are only shown for the reduced Brillouin zone $kT \in [0, \pi]$. It can be observed that as the wavenumber k increases, the frequency varies almost linearly with respect to k and hence the wave speed is almost constant over most of the interval; it is only towards the right boundary $kT = \pi$ that noticeable departure from these behaviors is observed. These behaviors have previously been noted by Norris et al. (2013) without prestress and their results have been used to validate our code. This flat behavior in v_s is explained by our asymptotic analysis in the next section.

As expected, the wave speed decreases monotonically as the stretch λ_1 is decreased and the trend shown by Fig. 4(b) seems to indicate the speed will first vanish at $kT = \pi$ when λ_1 is sufficiently small, but this turns out not to be the case. In Fig. 5 we display the variation of q_1, the smallest eigenvalue of $\boldsymbol{M}$, with respect to ω_s as λ_1 is decreased while kT is fixed at π. Since q_1 vanishing is equivalent to $\det \boldsymbol{M} = 0$ as far as the current computation of ω_s is concerned, the four plots in this figure show how the ω_s at $kT = \pi$ decreases to zero as λ_1 approaches a critical value approximately equal to 0.740. Similar plots are made for other values of kT and it is found that this critical value of λ_1 is actually independent of kT. This phenomenon is explained further in Section 5 by solving $\det \boldsymbol{M} = 0$ with $\omega_s = 0$ directly.

4. Asymptotic analysis

The formulation in the previous section breaks down when the wavenumber k is zero. This arises from the mathematical structure of the elastic matrices $\widetilde{\boldsymbol{Q}}$ and $\widetilde{\boldsymbol{R}}$, which contain terms of the form $k_n = k + g_n$ (where $g_n = 2\pi n/T$). When $k = 0$, the terms corresponding to $n = 0$ result in entire rows or columns of elements becoming zero, making direct solution impossible. To circumvent this difficulty, practical computations typically use the results for small values of k to extrapolate the result for $k = 0$. In this section, we derive an asymptotic expression for the frequency valid in the limit $k \to 0$. This analysis serves three purposes: yielding the homogenized properties of the periodic half-space, providing the frequency at $k = 0$ directly, and explaining the flat behavior in Fig. 4(b).

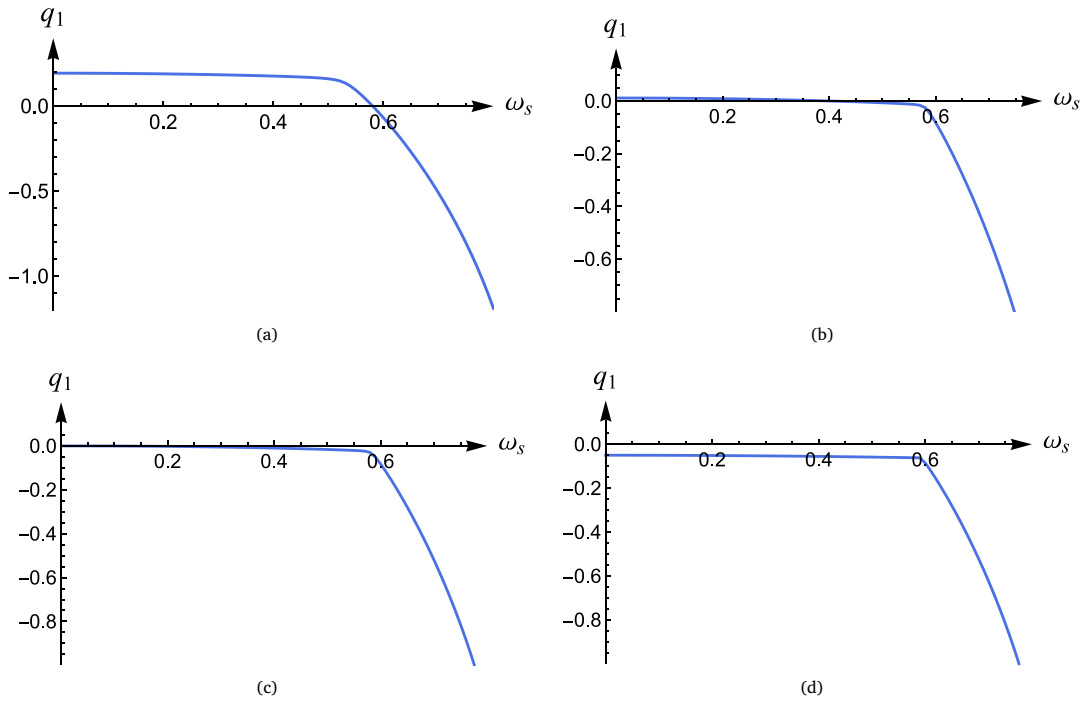


Fig. 5. Dependence of q_1 on ω_s as λ_1 is decreased. The intersection of each curve with the horizontal axis marks the frequency. These plots display the manner by which the frequency approaches zero. (a) $\lambda_1 = 0.741$; (b) $\lambda_1 = 0.7404$; (c) $\lambda_1 = 0.74037$; (d) $\lambda_1 = 0.7403$.

To ease interpretation, we replace $\mathcal{A}_{jilk}(x_1)$ and $\rho(x_1)$ in the previous section by $\mathcal{A}_{jilk}(x_1/T)$ and $\rho(x_1/T)$, respectively, so that $\mathcal{A}_{jilk}(\cdot)$ and $\rho(\cdot)$ are now 1-periodic functions of their argument. The incremental equation of motion then takes the form

$$\left(\mathcal{A}_{jilk}\left(\frac{x_1}{T}\right)u_{k,l}\right)_{,j} = -\omega^2\rho\left(\frac{x_1}{T}\right)u_i. \tag{4.1}$$

On making the substitutions

$$x_i \to Lx_i,\ u_i \to Lu_i,\ \mathcal{A}_{jilk} \to \mu_o\mathcal{A}_{jilk},\ \rho \to \rho_o\rho,\ \omega \to \sqrt{\frac{\mu_o}{\rho_o}}\frac{1}{L}\omega, \tag{4.2}$$

where L is a typical lengthscale of the same order as $1/k$, Eq. (4.1) takes the non-dimensionalized form

$$\frac{\partial}{\partial x_j}\left(\mathcal{A}_{jilk}(\xi)\frac{\partial u_k}{\partial x_l}\right) = -\omega^2\rho(\xi)u_i, \tag{4.3}$$

or equivalently,

$$\frac{\partial}{\partial x_1}\left\{\boldsymbol{Q}(\xi)\boldsymbol{u}_{,1} + \boldsymbol{R}(\xi)\boldsymbol{u}_{,2}\right\} + \boldsymbol{R}^T(\xi)\boldsymbol{u}_{,12} + \boldsymbol{T}(\xi)\boldsymbol{u}_{,22} = -\omega^2\boldsymbol{\rho}(\xi)\boldsymbol{u}, \tag{4.4}$$

where

$$\xi = x_1/\varepsilon, \qquad \varepsilon = T/L \ll 1.$$

According to the Floquet-Bloch theory, the displacement field admits a solution of the form

$$\boldsymbol{u}(x_1, x_2) = e^{\mathrm{i}kx_1}\boldsymbol{v}(\xi, x_2), \tag{4.5}$$

where the vector field $\boldsymbol{v}(\xi, x_2)$ is 1-periodic in terms of the first variable ξ.

4.1. The case of $k = O(1)$

Note that corresponding to the substitutions (4.2), the wavenumber k is subjected to the substitution $k \to k/L$ so that the kT in the previous section becomes $k\varepsilon$. Thus, under the assumptions $k = O(1)$ and $\varepsilon \ll 1$, we have $kT \ll 1$.

Since $\boldsymbol{u}$ depends on x_1 through both $e^{\mathrm{i}kx_1}$ and ξ, we have

$$\boldsymbol{u}_{,1} = \left\{\mathrm{i}k\boldsymbol{v} + \frac{1}{\epsilon}\boldsymbol{v}_{,\xi}\right\}e^{\mathrm{i}kx_1}, \qquad \boldsymbol{u}_{,2} = \boldsymbol{v}_{,2}e^{\mathrm{i}kx_1}, \tag{4.6}$$

and other higher order derivatives of $\boldsymbol{u}$ can be similarly obtained. On substituting these expressions into (4.4), we obtain

$$\frac{1}{\epsilon^2}(\boldsymbol{Q}\boldsymbol{v}_{,\xi})_{,\xi}+\frac{1}{\epsilon}\left\{(\boldsymbol{R}\boldsymbol{v}_{,2})_{,\xi}+\mathrm{i}k(\boldsymbol{Q}\boldsymbol{v})_{,\xi}+\boldsymbol{R}^T\boldsymbol{v}_{,\xi 2}+\mathrm{i}k\boldsymbol{Q}\boldsymbol{v}_{,\xi}\right\}$$
$$+\boldsymbol{T}\boldsymbol{v}_{,22}+\mathrm{i}k(\boldsymbol{R}+\boldsymbol{R}^T)\boldsymbol{v}_{,2}-(k^2\boldsymbol{Q}-\omega^2\rho)\boldsymbol{v}=\boldsymbol{0}. \tag{4.7}$$

The corresponding boundary conditions become

$$\frac{1}{\epsilon}\boldsymbol{R}^T\boldsymbol{v}_{,\xi}+\mathrm{i}k\boldsymbol{R}^T\boldsymbol{v}+\boldsymbol{T}\boldsymbol{v}_{,2}=\boldsymbol{0},\qquad x_2=0. \tag{4.8}$$

An asymptotic solution may then be sought in the form

$$\boldsymbol{v}=\boldsymbol{v}^{(0)}(x_2)+\varepsilon\boldsymbol{v}^{(1)}(\xi,x_2)+\epsilon^2\boldsymbol{v}^{(2)}(\xi,x_2)+\epsilon^3\boldsymbol{v}^{(3)}(\xi,x_2)+\epsilon^4\boldsymbol{v}^{(4)}(\xi,x_2)+\cdots, \tag{4.9a}$$
$$\omega=\omega_0+\epsilon^2\omega_1+\epsilon^4\omega_2+\cdots, \tag{4.9b}$$

where we have anticipated that the leading order term $\boldsymbol{v}^{(0)}(x_2)$ should be independent of the fast variable ξ. Inherited from $\boldsymbol{v}$, all the other functions in (4.9a) and their derivatives are 1-periodic in ξ.

On substituting (4.9a) and (4.9b) into Eq. (4.7), and equating the coefficients of ϵ^{-1}, ϵ^0, ϵ, and ϵ^2, we obtain

$$(\boldsymbol{Q}\boldsymbol{v}^{(1)}_{,\xi}+\boldsymbol{R}\boldsymbol{v}^{(0)}_{,2}+\mathrm{i}k\boldsymbol{Q}\boldsymbol{v}^{(0)})_{,\xi}=\boldsymbol{0}, \tag{4.10a}$$
$$(\boldsymbol{Q}\boldsymbol{v}^{(2)}_{,\xi}+\boldsymbol{R}\boldsymbol{v}^{(1)}_{,2}+\mathrm{i}k\boldsymbol{Q}\boldsymbol{v}^{(1)})_{,\xi}+\mathcal{J}[\boldsymbol{v}^{(1)}_{,\xi}]+\mathcal{L}[\boldsymbol{v}^{(0)}]=\boldsymbol{0}, \tag{4.10b}$$
$$(\boldsymbol{Q}\boldsymbol{v}^{(3)}_{,\xi}+\boldsymbol{R}\boldsymbol{v}^{(2)}_{,2}+\mathrm{i}k\boldsymbol{Q}\boldsymbol{v}^{(2)})_{,\xi}+\mathcal{J}[\boldsymbol{v}^{(2)}_{,\xi}]+\mathcal{L}[\boldsymbol{v}^{(1)}]=\boldsymbol{0}, \tag{4.10c}$$
$$(\boldsymbol{Q}\boldsymbol{v}^{(4)}_{,\xi}+\boldsymbol{R}\boldsymbol{v}^{(3)}_{,2}+\mathrm{i}k\boldsymbol{Q}\boldsymbol{v}^{(3)})_{,\xi}+\mathcal{J}[\boldsymbol{v}^{(3)}_{,\xi}]+\mathcal{L}[\boldsymbol{v}^{(2)}]+2\omega_0\omega_1\rho\boldsymbol{v}^{(0)}=\boldsymbol{0}, \tag{4.10d}$$

whereas substitution of (4.9a) into the boundary conditions (4.8) yields

$$\boldsymbol{R}^T\boldsymbol{v}^{(1)}_{,\xi}+\mathcal{B}[\boldsymbol{v}^{(0)}]=\boldsymbol{0},\qquad x_2=0, \tag{4.11a}$$
$$\boldsymbol{R}^T\boldsymbol{v}^{(2)}_{,\xi}+\mathcal{B}[\boldsymbol{v}^{(1)}]=\boldsymbol{0},\qquad x_2=0, \tag{4.11b}$$
$$\boldsymbol{R}^T\boldsymbol{v}^{(3)}_{,\xi}+\mathcal{B}[\boldsymbol{v}^{(2)}]=\boldsymbol{0},\qquad x_2=0. \tag{4.11c}$$

In the above expressions, the differential operators $\mathcal{L}$, $\mathcal{J}$, and $\mathcal{B}$ are defined by

$$\mathcal{L}[\boldsymbol{v}]=\boldsymbol{T}\boldsymbol{v}_{,22}+\mathrm{i}k(\boldsymbol{R}+\boldsymbol{R}^T)\boldsymbol{v}_{,2}-(k^2\boldsymbol{Q}-\omega_0^2\rho)\boldsymbol{v}, \tag{4.12a}$$
$$\mathcal{J}[\boldsymbol{v}]=\boldsymbol{R}^T\boldsymbol{v}_{,2}+\mathrm{i}k\boldsymbol{Q}\boldsymbol{v}, \tag{4.12b}$$
$$\mathcal{B}[\boldsymbol{v}]=\mathrm{i}k\boldsymbol{R}^T\boldsymbol{v}+\boldsymbol{T}\boldsymbol{v}_{,2}. \tag{4.12c}$$

Eqs. (4.10a) – (4.10c) can each be integrated once to give

$$\boldsymbol{Q}\boldsymbol{v}^{(1)}_{,\xi}+\boldsymbol{R}\boldsymbol{v}^{(0)}_{,2}+\mathrm{i}k\boldsymbol{Q}\boldsymbol{v}^{(0)}=\boldsymbol{c}(x_2), \tag{4.13a}$$
$$\boldsymbol{Q}\boldsymbol{v}^{(2)}_{,\xi}+\boldsymbol{R}\boldsymbol{v}^{(1)}_{,2}+\mathrm{i}k\boldsymbol{Q}\boldsymbol{v}^{(1)}+\int_0^\xi(\mathcal{J}[\boldsymbol{v}^{(1)}_{,\xi}]+\mathcal{L}[\boldsymbol{v}^{(0)}])d\xi=\boldsymbol{e}(x_2), \tag{4.13b}$$
$$\boldsymbol{Q}\boldsymbol{v}^{(3)}_{,\xi}+\boldsymbol{R}\boldsymbol{v}^{(2)}_{,2}+\mathrm{i}k\boldsymbol{Q}\boldsymbol{v}^{(2)}+\int_0^\xi(\mathcal{J}[\boldsymbol{v}^{(2)}_{,\xi}]+\mathcal{L}[\boldsymbol{v}^{(1)}])d\xi=\boldsymbol{g}(x_2), \tag{4.13c}$$

where the functions $\boldsymbol{c}(x_2),\boldsymbol{e}(x_2),\boldsymbol{g}(x_2)$ arising from integration can be determined by multiplying each of the above equations by $\boldsymbol{Q}^{-1}$ and then averaging over a unit cell:

$$\boldsymbol{c}(x_2)=\mathcal{M}[\boldsymbol{v}^{(0)}], \tag{4.14a}$$
$$\boldsymbol{e}(x_2)=\mathcal{M}[\boldsymbol{v}^{(1)}]+\breve{\boldsymbol{Q}}\langle\boldsymbol{Q}^{-1}\int_0^\xi(\mathcal{J}[\boldsymbol{v}^{(1)}_{,\xi}]+\mathcal{L}[\boldsymbol{v}^{(0)}])d\xi\rangle, \tag{4.14b}$$
$$\boldsymbol{g}(x_2)=\mathcal{M}[\boldsymbol{v}^{(2)}]+\breve{\boldsymbol{Q}}\langle\boldsymbol{Q}^{-1}\int_0^\xi(\mathcal{J}[\boldsymbol{v}^{(2)}_{,\xi}]+\mathcal{L}[\boldsymbol{v}^{(1)}])d\xi\rangle. \tag{4.14c}$$

where each pair of angle brackets signifies the above-mentioned averaging and the operator $\mathcal{M}$ and matrix $\breve{\boldsymbol{Q}}$ are defined by

$$\mathcal{M}[\boldsymbol{v}]=\breve{\boldsymbol{Q}}\langle\boldsymbol{Q}^{-1}\boldsymbol{R}\boldsymbol{v}_{,2}\rangle+\mathrm{i}k\breve{Q}\langle\boldsymbol{v}\rangle,\qquad \breve{\boldsymbol{Q}}=\langle\boldsymbol{Q}^{-1}\rangle^{-1}=\left(\int_0^1\boldsymbol{Q}^{-1}d\xi\right)^{-1}. \tag{4.15}$$

On the other hand, on multiplying each of the three Eqs. (4.13a), (4.13b), and (4.13c) by $\boldsymbol{Q}^{-1}$ and then integrating, we obtain

$$\boldsymbol{v}^{(1)}(\xi,x_2)=\tilde{\boldsymbol{v}}^{(1)}(\xi,x_2)+\boldsymbol{v}^{(01)}(x_2), \tag{4.16a}$$
$$\boldsymbol{v}^{(2)}(\xi,x_2)=\tilde{\boldsymbol{v}}^{(2)}(\xi,x_2)+\boldsymbol{v}^{(02)}(x_2), \tag{4.16b}$$

$$\boldsymbol{v}^{(3)}(\xi, x_2) = \tilde{\boldsymbol{v}}^{(3)}(\xi, x_2) + \boldsymbol{v}^{(03)}(x_2), \tag{4.16c}$$

where $\boldsymbol{v}^{(01)}(x_2), \boldsymbol{v}^{(02)}(x_2), \boldsymbol{v}^{(03)}(x_2)$ are arbitrary functions and

$$\tilde{\boldsymbol{v}}^{(1)}(\xi, x_2) = \left(\int_0^\xi \boldsymbol{Q}^{-1} d\xi\right)\boldsymbol{c}(x_2) - \int_0^\xi \boldsymbol{Q}^{-1}\boldsymbol{R}\boldsymbol{v}^{(0)}_{,2} d\xi - \mathrm{i}k\xi\boldsymbol{v}^{(0)}, \tag{4.17a}$$

$$\begin{aligned}\tilde{\boldsymbol{v}}^{(2)}(\xi, x_2) = &\left(\int_0^\xi \boldsymbol{Q}^{-1} d\xi\right)\boldsymbol{e}(x_2) - \int_0^\xi \boldsymbol{Q}^{-1}\boldsymbol{R}\boldsymbol{v}^{(1)}_{,2} d\xi - \mathrm{i}k\int_0^\xi \boldsymbol{v}^{(1)} d\xi \\ &- \int_0^\xi \left\{\boldsymbol{Q}^{-1}\int_0^\xi (\mathcal{J}[\boldsymbol{v}^{(1)}_{,\xi}] + \mathcal{L}[\boldsymbol{v}^{(0)}]) d\xi\right\} d\xi,\end{aligned} \tag{4.17b}$$

$$\begin{aligned}\tilde{\boldsymbol{v}}^{(3)}(\xi, x_2) = &\left(\int_0^\xi \boldsymbol{Q}^{-1} d\xi\right)\boldsymbol{g}(x_2) - \int_0^\xi \boldsymbol{Q}^{-1}\boldsymbol{R}\boldsymbol{v}^{(2)}_{,2} d\xi - \mathrm{i}k\int_0^\xi \boldsymbol{v}^{(2)} d\xi \\ &- \int_0^\xi \left\{\boldsymbol{Q}^{-1}\int_0^\xi (\mathcal{J}[\boldsymbol{v}^{(2)}_{,\xi}] + \mathcal{L}[\boldsymbol{v}^{(1)}]) d\xi\right\} d\xi.\end{aligned} \tag{4.17c}$$

Integrating Eqs. (4.10b)–(4.10d) over a period in ξ and making use of the expressions (4.16a)–(4.16c), we obtain

$$\langle \mathcal{J}[\tilde{\boldsymbol{v}}^{(1)}_{,\xi}] + \mathcal{L}[\boldsymbol{v}^{(0)}]\rangle = \boldsymbol{0}, \tag{4.18a}$$

$$\langle \mathcal{J}[\tilde{\boldsymbol{v}}^{(2)}_{,\xi}] + \mathcal{L}[\tilde{\boldsymbol{v}}^{(1)}] + \mathcal{L}[\boldsymbol{v}^{(01)}]\rangle = \boldsymbol{0}, \tag{4.18b}$$

$$\langle \mathcal{J}[\tilde{\boldsymbol{v}}^{(3)}_{,\xi}] + \mathcal{L}[\tilde{\boldsymbol{v}}^{(2)}] + \mathcal{L}[\boldsymbol{v}^{(02)}]\rangle + 2\omega_0\omega_1\langle\boldsymbol{\rho}\rangle\boldsymbol{v}^{(0)} = \boldsymbol{0}. \tag{4.18c}$$

These three equations are to be solved subject to three boundary conditions that are the averages of (4.11a), (4.11b), and (4.11c):

$$\langle \boldsymbol{R}^T\tilde{\boldsymbol{v}}^{(1)}_{,\xi}\rangle + \langle \mathcal{B}[\boldsymbol{v}^{(0)}]\rangle = \boldsymbol{0}, \qquad x_2 = 0, \tag{4.19a}$$

$$\langle \boldsymbol{R}^T\tilde{\boldsymbol{v}}^{(2)}_{,\xi} + \mathcal{B}[\tilde{\boldsymbol{v}}^{(1)}]\rangle + \langle \mathcal{B}[\boldsymbol{v}^{(01)}]\rangle = \boldsymbol{0}, \qquad x_2 = 0, \tag{4.19b}$$

$$\langle \boldsymbol{R}^T\tilde{\boldsymbol{v}}^{(3)}_{,\xi} + \mathcal{B}[\tilde{\boldsymbol{v}}^{(2)}]\rangle + \langle \mathcal{B}[\boldsymbol{v}^{(02)}]\rangle = \boldsymbol{0}, \qquad x_2 = 0. \tag{4.19c}$$

It will now be shown that (i) Eq. (4.18a) subject to the boundary condition (4.19a) can be converted into a surface wave problem for a homogenized half-space that determines ω_0, (ii) Eq. (4.18b) subject to (4.19b) may be solved to find $\boldsymbol{v}^{(01)}$, and (iii) Eq. (4.18c) subject to (4.19c) can be solved only if a solvability condition is imposed and this solvability condition provides a linear equation for finding the leading-order correction ω_1.

First, substituting the expression for $\tilde{\boldsymbol{v}}^{(1)}$ from Eq. (4.17a) into the first-order equation (4.18a) yields

$$\begin{aligned}&\langle \boldsymbol{R}^T\{\boldsymbol{Q}^{-1}\mathcal{M}[\boldsymbol{v}^{(0)}_{,2}] - \boldsymbol{Q}^{-1}\boldsymbol{R}\boldsymbol{v}^{(0)}_{,22} - \mathrm{i}k\boldsymbol{v}^{(0)}_{,2}\} + \mathrm{i}k\boldsymbol{Q}\{\boldsymbol{Q}^{-1}\mathcal{M}[\boldsymbol{v}^{(0)}] - \boldsymbol{Q}^{-1}\boldsymbol{R}\boldsymbol{v}^{(0)}_{,2} - \mathrm{i}k\boldsymbol{v}^{(0)}\}\rangle \\ &+\langle\boldsymbol{T}\rangle\boldsymbol{v}^{(0)}_{,22} + \mathrm{i}k\langle\boldsymbol{R} + \boldsymbol{R}^T\rangle\boldsymbol{v}^{(0)}_{,2} - (k^2\langle\boldsymbol{Q}\rangle - \omega_0^2\langle\boldsymbol{\rho}\rangle)\boldsymbol{v}^{(0)} = \boldsymbol{0}.\end{aligned} \tag{4.20}$$

Further simplification leads to

$$\bar{\mathcal{L}}[\boldsymbol{v}^{(0)}] \equiv \bar{\boldsymbol{T}}\boldsymbol{v}^{(0)}_{,22} + \mathrm{i}k(\bar{\boldsymbol{R}} + \bar{\boldsymbol{R}}^T)\boldsymbol{v}^{(0)}_{,2} - (k^2\bar{\boldsymbol{Q}} - \omega_0^2\langle\boldsymbol{\rho}\rangle)\boldsymbol{v}^{(0)} = \boldsymbol{0}, \tag{4.21}$$

where the first equation defines the homogenized operator $\bar{\mathcal{L}}$ and

$$\bar{\boldsymbol{Q}} = \check{\boldsymbol{Q}}, \qquad \bar{\boldsymbol{T}} = \langle\boldsymbol{T}\rangle - \langle\boldsymbol{R}^T\boldsymbol{Q}^{-1}\boldsymbol{R}\rangle + \langle\boldsymbol{R}^T\boldsymbol{Q}^{-1}\rangle\check{\boldsymbol{Q}}\langle\boldsymbol{Q}^{-1}\boldsymbol{R}\rangle, \qquad \bar{\boldsymbol{R}} = \check{\boldsymbol{Q}}\langle\boldsymbol{Q}^{-1}\boldsymbol{R}\rangle. \tag{4.22}$$

The associated homogenized boundary condition can be obtained by substituting the expression (4.17a) into (4.19a), which gives, after simplification,

$$\bar{\mathcal{B}}[\boldsymbol{v}^{(0)}] \equiv \mathrm{i}k\bar{\boldsymbol{R}}^T\boldsymbol{v}^{(0)} + \bar{\boldsymbol{T}}\boldsymbol{v}^{(0)}_{,2} = \boldsymbol{0}, \qquad x_2 = 0, \tag{4.23}$$

where the first equation defines the homogenized operator $\bar{\mathcal{B}}$.

The homogenized surface wave problem of (4.21) subject to the boundary condition (4.23) take the same form as the surface wave problem (3.6a) and (3.6b) for a homogeneous half-space. Thus, its solution, in particular the surface wave speed, can be determined using the method outlined there.

We next solve the second order problem of (4.18b) subject to (4.19b) and the third order problem of (4.18c) subject to (4.19c). To manipulate these equations into a more transparent form, we first rewriting Eqs. (4.14a)–(4.14c) as

$$\boldsymbol{c}(x_2) = \mathcal{M}[\boldsymbol{v}^{(0)}], \qquad \boldsymbol{e}(x_2) = \mathcal{M}[\boldsymbol{v}^{(01)}] + \tilde{\boldsymbol{e}}(x_2), \qquad \boldsymbol{g}(x_2) = \mathcal{M}[\boldsymbol{v}^{(02)}] + \tilde{\boldsymbol{g}}(x_2), \tag{4.24}$$

where

$$\begin{aligned}\tilde{\boldsymbol{e}}(x_2) &= \mathcal{M}[\tilde{\boldsymbol{v}}^{(1)}] + \check{\boldsymbol{Q}}\langle\boldsymbol{Q}^{-1}\int_0^\xi (\mathcal{J}[\tilde{\boldsymbol{v}}^{(1)}_{,\xi}] + \mathcal{L}[\boldsymbol{v}^{(0)}]) d\xi\rangle, \\ \tilde{\boldsymbol{g}}(x_2) &= \mathcal{M}[\tilde{\boldsymbol{v}}^{(2)}] + \check{\boldsymbol{Q}}\langle\boldsymbol{Q}^{-1}\int_0^\xi (\mathcal{J}[\tilde{\boldsymbol{v}}^{(2)}_{,\xi}] + \mathcal{L}[\tilde{\boldsymbol{v}}^{(1)}] + \mathcal{L}[\boldsymbol{v}^{(01)}]) d\xi\rangle.\end{aligned} \tag{4.25}$$

The three derivatives $\tilde{\boldsymbol{v}}^{(1)}_{,\xi}$, $\tilde{\boldsymbol{v}}^{(2)}_{,\xi}$ and $\tilde{\boldsymbol{v}}^{(3)}_{,\xi}$ in the equations to be solved can be obtained from (4.17a)–(4.17c) as follows:

$$\tilde{\boldsymbol{v}}^{(1)}_{,\xi} = \boldsymbol{Q}^{-1}\mathcal{M}[\boldsymbol{v}^{(0)}] - \boldsymbol{Q}^{-1}\boldsymbol{R}\boldsymbol{v}^{(0)}_{,2} - \mathrm{i}k\boldsymbol{v}^{(0)}, \tag{4.26a}$$

$$\tilde{\boldsymbol{v}}^{(2)}_{,\xi} = \boldsymbol{Q}^{-1}\mathcal{M}[\boldsymbol{v}^{(01)}] - \boldsymbol{Q}^{-1}\boldsymbol{R}\boldsymbol{v}^{(01)}_{,2} - \mathrm{i}k\boldsymbol{v}^{(01)} + \tilde{\boldsymbol{v}}^{(2)}_{,\xi}, \tag{4.26b}$$

$$\tilde{\boldsymbol{v}}^{(3)}_{,\xi} = \boldsymbol{Q}^{-1}\mathcal{M}[\boldsymbol{v}^{(02)}] - \boldsymbol{Q}^{-1}\boldsymbol{R}\boldsymbol{v}^{(02)}_{,2} - \mathrm{i}k\boldsymbol{v}^{(02)} + \tilde{\boldsymbol{v}}^{(3)}_{,\xi}, \tag{4.26c}$$

where

$$\tilde{\boldsymbol{v}}^{(2)}_{,\xi} = \boldsymbol{Q}^{-1}\tilde{\boldsymbol{e}}(x_2) - \boldsymbol{Q}^{-1}\int_0^{\xi}(\mathcal{J}[\tilde{\boldsymbol{v}}^{(1)}_{,\xi}] + \mathcal{L}[\boldsymbol{v}^{(0)}])d\xi - \boldsymbol{Q}^{-1}\boldsymbol{R}\tilde{\boldsymbol{v}}^{(1)}_{,2} - \mathrm{i}k\tilde{\boldsymbol{v}}^{(1)}, \tag{4.27a}$$

$$\tilde{\boldsymbol{v}}^{(3)}_{,\xi} = \boldsymbol{Q}^{-1}\tilde{\boldsymbol{g}}(x_2) - \boldsymbol{Q}^{-1}\int_0^{\xi}(\mathcal{J}[\tilde{\boldsymbol{v}}^{(2)}_{,\xi}] + \mathcal{L}[\boldsymbol{v}^{(1)}])d\xi - \boldsymbol{Q}^{-1}\boldsymbol{R}\tilde{\boldsymbol{v}}^{(2)}_{,2} - \mathrm{i}k\tilde{\boldsymbol{v}}^{(2)}. \tag{4.27b}$$

With the use of these expressions, we find that $\boldsymbol{v}^{(01)}$ appears in (4.18b) and $\boldsymbol{v}^{(02)}$ appears in (4.18c) in the same form as $\boldsymbol{v}^{(0)}$ appears in (4.20), thus obtaining

$$\bar{\mathcal{L}}[\boldsymbol{v}^{(01)}] = -\langle \boldsymbol{R}^T\tilde{\boldsymbol{v}}^{(2)}_{,\xi 2} + \mathrm{i}k\boldsymbol{Q}\tilde{\boldsymbol{v}}^{(2)}_{,\xi} + \mathcal{L}[\tilde{\boldsymbol{v}}^{(1)}]\rangle, \tag{4.28a}$$

$$\bar{\mathcal{L}}[\boldsymbol{v}^{(02)}] = -\langle \boldsymbol{R}^T\tilde{\boldsymbol{v}}^{(3)}_{,\xi 2} + \mathrm{i}k\boldsymbol{Q}\tilde{\boldsymbol{v}}^{(3)}_{,\xi} + \mathcal{L}[\tilde{\boldsymbol{v}}^{(2)}]\rangle - 2\omega_0\omega_1\langle\boldsymbol{\rho}\rangle\boldsymbol{v}^{(0)}. \tag{4.28b}$$

Similar simplifications can be made to reduce the two boundary conditions (4.19b) and (4.19c) to

$$\bar{\mathcal{B}}[\boldsymbol{v}^{(01)}] = -\langle \boldsymbol{R}^T\tilde{\boldsymbol{v}}^{(2)}_{,\xi}\rangle - \langle\mathcal{B}[\tilde{\boldsymbol{v}}^{(1)}]\rangle, \qquad x_2 = 0, \tag{4.29a}$$

$$\bar{\mathcal{B}}[\boldsymbol{v}^{(02)}] = -\langle \boldsymbol{R}^T\tilde{\boldsymbol{v}}^{(3)}_{,\xi}\rangle - \langle\mathcal{B}[\tilde{\boldsymbol{v}}^{(2)}]\rangle, \qquad x_2 = 0. \tag{4.29b}$$

Because it is known from earlier discussion that the differential equation $\bar{\mathcal{L}}[\boldsymbol{v}] = 0$, subjected to the boundary condition $\bar{\mathcal{B}}[\boldsymbol{v}] = 0$ on $x_2 = 0$ and the decaying condition $\boldsymbol{v} \to 0$ as $x_2 \to \infty$, has a non-trivial solution, $\boldsymbol{v} = \boldsymbol{v}^{(0)}$ say, the right hand sides of (4.28a)–(4.29b) must satisfy two solvability conditions. The solvability conditions are obtained by noting that the operators $\bar{\mathcal{L}}$ and $\bar{\mathcal{B}}$ enjoy the property

$$\int_0^{\infty}\bar{\boldsymbol{v}}^{(0)}\cdot\bar{\mathcal{L}}[\boldsymbol{v}]\mathrm{d}x_2 = (\bar{\boldsymbol{v}}^{(0)}\cdot\bar{\mathcal{B}}[\boldsymbol{v}])|_0^{\infty}, \quad \forall\boldsymbol{v}, \tag{4.30}$$

where $\bar{\boldsymbol{v}}^{(0)}$ denotes the complex conjugate of $\boldsymbol{v}^{(0)}$. This identity can be verified by integration by parts repeatedly, followed by the use of the fact that $\boldsymbol{v}^{(0)}$ is the above-mentioned non-trivial solution; see Fu and Mielke (2002).

Replacing $\boldsymbol{v}$ by $\boldsymbol{v}^{(01)}$ in (4.30) and substituting in (4.28a) and (4.29a), we verify numerically that the solvability condition is satisfied automatically. This is anticipated since there is no disposable parameter in this equation. However, on replacing $\boldsymbol{v}$ by $\boldsymbol{v}^{(02)}$ in (4.30) and substituting in (4.28b) and (4.29b), we find $\omega_1 = c_1k^3$, where c_1 is a constant whose expression is not written out here for brevity but is evaluated with the aid of the symbolic manipulation package *Mathematica*. Substituting this back into the expansion (4.9b) yields

$$\omega = \omega_0 + \epsilon^2 c_1 k^3 + \cdots.$$

Making substitutions reversing those in (4.2) together with $k \to kL$, we obtain

$$\omega = k\bar{v} + \sqrt{\mu_o/\rho_o}\,c_1k(kT)^2 + \cdots, \tag{4.31}$$

where, for instance, ω is the actual (i.e. dimensional) angular frequency and $\bar{v}$ is the actual surface wave speed associated with the homogenized half-space. The actual wave speed is then given by $v = \omega/k$.

Eq. (4.31) will be used in its non-dimensional form given by

$$\omega_s = \omega T/v_o = kT\bar{v}/v_o + c_1(kT)^3 + \cdots, \tag{4.32}$$

together with $v_s = \omega_s/(kT)$ for the non-dimensional wave speed. The above expansion procedure can be carried out to higher orders. The next correction term would be of order $(kT)^5$, but we do not present the details for the sake of brevity.

As an illustration, for $\lambda_1 = 1$ and $\lambda_1 = 0.8$ our asymptotic analysis yields, respectively,

$$\begin{aligned} v_s|_{\lambda_1=1} &= 1.114 + 0.001683\,(kT)^2 + 0.001564\,(kT)^4 + \cdots, \\ v_s|_{\lambda_1=0.8} &= 0.7561 + 0.004011\,(kT)^2 - 0.003932\,(kT)^4 + \cdots. \end{aligned} \tag{4.33}$$

It is seen that the coefficients of the two correction terms are quite small, which explains the flat behavior of v_s over most of the Brillouin zone. These asymptotic solutions are compared with the theoretical solutions of Section 3 in Fig. 6, where the solid lines represent the theoretical solutions and the red dashed lines denote the asymptotic solutions. It can be observed that the asymptotic solutions agree well with the theoretical solutions when $kT \ll 1$ and the two solutions begin to diverge from each other only when kT has become as large as 2.

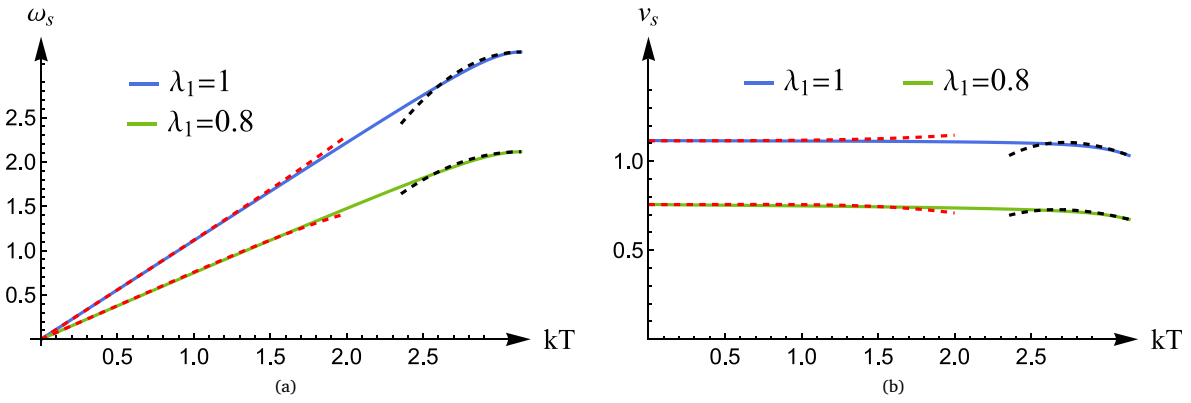


Fig. 6. Comparison between asymptotic and exact results for two representative values of pre-stretch when $\alpha = 2$ and $\delta = 0.5$.

4.2. The case of $k = O(1/\epsilon)$

For completeness, we now also consider k in a small neighborhood of the right end $k = \pi/\epsilon$ of the Brillouin zone and write

$$k = \frac{\pi}{\epsilon} + k_1 = k_0 + k_1,$$

where $k_0 = \pi/\epsilon$ and k_1 is an $O(1)$ constant representing the deviation of k from k_0. The Floquet-Bloch solution (4.5) can then be rewritten in the form

$$\boldsymbol{u}(x_1, x_2) = e^{\mathrm{i}k_1 x_1} e^{\mathrm{i}\pi\xi} \boldsymbol{v}(\xi, \eta) = e^{\mathrm{i}k_1 x_1} \hat{\boldsymbol{v}}(\xi, \eta), \qquad \eta = \frac{x_2}{\epsilon}, \tag{4.34}$$

where $\hat{\boldsymbol{v}}(\xi, \eta) = e^{\mathrm{i}\pi\xi} \boldsymbol{v}(\xi, \eta)$. Note that the dependence on x_2 is now through the new scaled variable η since we expect that dependence of our solution on the two spatial variables should be on the same lengthscale. Note also that $\hat{\boldsymbol{v}}(\xi, \eta)$ is not 1-periodic in ξ; instead, it has the property

$$\hat{\boldsymbol{v}}(\xi + 1, \eta) = e^{\mathrm{i}\pi} e^{\mathrm{i}\pi\xi} \boldsymbol{v}(\xi + 1, \eta) = -\hat{\boldsymbol{v}}(\xi, \eta). \tag{4.35}$$

For easy reference, we shall refer to any function satisfying the above property as being anti-periodic. The methodology employed in this subsection has previously been used by Craster et al. (2010) and Craster et al. (2012) under the name of high-frequency homogenization, but its origin can be traced at least back to Newell (1974) where the introduction of an extra stretched variable was used in a multiple-scale analysis to study the modulation of nonlinear waves.

On substituting (4.34) into (4.4), noting, for instance,

$$\boldsymbol{u}_{,1} = \left\{ \mathrm{i}k_1 \hat{\boldsymbol{v}} + \frac{1}{\epsilon} \hat{\boldsymbol{v}}_{,\xi} \right\} e^{\mathrm{i}k_1 x_1}, \qquad \boldsymbol{u}_{,2} = \frac{1}{\epsilon} \hat{\boldsymbol{v}}_{,\eta} e^{\mathrm{i}k_1 x_1}, \tag{4.36}$$

we obtain

$$\begin{aligned} &\frac{1}{\epsilon^2} \left\{ (\boldsymbol{Q}\hat{\boldsymbol{v}}_{,\xi})_{,\xi} + (\boldsymbol{R}\hat{\boldsymbol{v}}_{,\eta})_{,\xi} + \boldsymbol{R}^T \hat{\boldsymbol{v}}_{,\xi\eta} + \boldsymbol{T}\hat{\boldsymbol{v}}_{,\eta\eta} \right\} \\ &+ \frac{1}{\epsilon} \left\{ \mathrm{i}k_1 (\boldsymbol{Q}\hat{\boldsymbol{v}})_{,\xi} + \mathrm{i}k_1 \boldsymbol{Q}\hat{\boldsymbol{v}}_{,\xi} + \mathrm{i}k_1 (\boldsymbol{R} + \boldsymbol{R}^T)\hat{\boldsymbol{v}}_{,\eta} \right\} - (k_1^2 \boldsymbol{Q} - \rho\omega^2 \boldsymbol{I})\hat{\boldsymbol{v}} = \boldsymbol{0}. \end{aligned} \tag{4.37}$$

The corresponding boundary conditions become

$$\frac{1}{\epsilon} \left\{ \boldsymbol{R}^T \hat{\boldsymbol{v}}_{,\xi} + \boldsymbol{T}\hat{\boldsymbol{v}}_{,\eta} \right\} + \mathrm{i}k_1 \boldsymbol{R}^T \hat{\boldsymbol{v}} = \boldsymbol{0}, \qquad \eta = 0. \tag{4.38}$$

An asymptotic solution can then be sought in the form

$$\hat{\boldsymbol{v}} = \hat{\boldsymbol{v}}^{(0)}(\xi, \eta) + \epsilon \hat{\boldsymbol{v}}^{(1)}(\xi, \eta) + \epsilon^2 \hat{\boldsymbol{v}}^{(2)}(\xi, \eta) + \epsilon^3 \hat{\boldsymbol{v}}^{(3)}(\xi, \eta) + \epsilon^4 \hat{\boldsymbol{v}}^{(4)}(\xi, \eta) + \cdots, \tag{4.39a}$$

$$\omega = \frac{1}{\epsilon} \left\{ \omega_0 + \epsilon^2 \omega_1 + \epsilon^4 \omega_2 + \cdots \right\}, \tag{4.39b}$$

where it is noted that the leading order term $\hat{\boldsymbol{v}}^{(0)}(\xi, \eta)$ is no longer independent of the fast variable ξ. Inherited from $\hat{\boldsymbol{v}}$, all the functions on the right hand side of (4.39a) and their derivatives are anti-periodic in terms of ξ.

On substituting (4.39a) and (4.39b) into Eq. (4.37), and equating the coefficients of ϵ^{-2}, ϵ^{-1}, ϵ^0, we obtain

$$\hat{\mathcal{L}}[\hat{\boldsymbol{v}}^{(0)}] = \boldsymbol{0}, \tag{4.40a}$$

$$\hat{\mathcal{L}}[\hat{\boldsymbol{v}}^{(1)}] + \mathrm{i}k_1 (\boldsymbol{Q}\hat{\boldsymbol{v}}^{(0)})_{,\xi} + \mathrm{i}k_1 \boldsymbol{Q}\hat{\boldsymbol{v}}^{(0)}_{,\xi} + \mathrm{i}k_1 (\boldsymbol{R} + \boldsymbol{R}^T)\hat{\boldsymbol{v}}^{(0)}_{,\eta} = \boldsymbol{0}, \tag{4.40b}$$

$$\hat{\mathcal{L}}[\hat{\boldsymbol{v}}^{(2)}] + \mathrm{i}k_1(\boldsymbol{Q}\hat{\boldsymbol{v}}^{(1)})_{,\xi} + \mathrm{i}k_1\boldsymbol{Q}\hat{\boldsymbol{v}}^{(1)}_{,\xi} + \mathrm{i}k_1(\boldsymbol{R}+\boldsymbol{R}^T)\hat{\boldsymbol{v}}^{(1)}_{,\eta} + (2\rho\omega_0\omega_1\boldsymbol{I} - k_1^2\boldsymbol{Q})\hat{\boldsymbol{v}}^{(0)} = \boldsymbol{0}, \tag{4.40c}$$

where the new operator $\hat{\mathcal{L}}$ is defined by

$$\hat{\mathcal{L}}[\hat{\boldsymbol{v}}] = (\boldsymbol{Q}\hat{\boldsymbol{v}}_{,\xi})_{,\xi} + (\boldsymbol{R}\hat{\boldsymbol{v}}_{,\eta})_{,\xi} + \boldsymbol{R}^T\hat{\boldsymbol{v}}_{,\xi\eta} + \boldsymbol{T}\hat{\boldsymbol{v}}_{,\eta\eta} + \rho\omega_0^2\hat{\boldsymbol{v}}. \tag{4.41}$$

The boundary conditions (4.38) yield

$$\hat{\mathcal{B}}[\hat{\boldsymbol{v}}^{(0)}] = \boldsymbol{0}, \qquad x_2 = 0, \tag{4.42a}$$

$$\hat{\mathcal{B}}[\hat{\boldsymbol{v}}^{(1)}] + \mathrm{i}k_1\boldsymbol{R}^T\hat{\boldsymbol{v}}^{(0)} = \boldsymbol{0}, \qquad x_2 = 0, \tag{4.42b}$$

$$\hat{\mathcal{B}}[\hat{\boldsymbol{v}}^{(2)}] + \mathrm{i}k_1\boldsymbol{R}^T\hat{\boldsymbol{v}}^{(1)} = \boldsymbol{0}, \qquad x_2 = 0, \tag{4.42c}$$

where the new operator $\hat{\mathcal{B}}$ is defined by

$$\hat{\mathcal{B}}[\hat{\boldsymbol{v}}] = \boldsymbol{R}^T\hat{\boldsymbol{v}}_{,\xi} + \boldsymbol{T}\hat{\boldsymbol{v}}_{,\eta}. \tag{4.43}$$

It is seen that the operators $\hat{\mathcal{L}}$ and $\hat{\mathcal{B}}$ reduce to $\mathcal{L}$ and $\mathcal{B}$ for a homogeneous half-space.

Eq. (4.40a) subjected to the boundary condition (4.42a) and the decaying condition $\hat{\boldsymbol{v}}^{(0)} \to 0$ as $x_2 \to \infty$ is a boundary value problem defined on a unit cell that can only be solved numerically to find ω_0 and $\hat{\boldsymbol{v}}^{(0)}$ up to an arbitrary constant. The next-order boundary value problem for $\hat{\boldsymbol{v}}^{(1)}$ is inhomogeneous, and has a particular solution given by $\hat{\boldsymbol{v}}^{(1)} = -\mathrm{i}k_1\xi\hat{\boldsymbol{v}}^{(0)}$. Thus, the general solution is given by

$$\hat{\boldsymbol{v}}^{(1)} = \mathrm{i}k_1\left\{\hat{\boldsymbol{v}}^{(10)} - \xi\hat{\boldsymbol{v}}^{(0)}\right\}, \tag{4.44}$$

where $\hat{\boldsymbol{v}}^{(10)}$ is a *forced* solution of (4.40a) and (4.42a) such that the $\hat{\boldsymbol{v}}^{(1)}$ given by (4.44) is anti-periodic in ξ, or equivalently,

$$\hat{\boldsymbol{v}}^{(10)}(1,\eta) = -\hat{\boldsymbol{v}}^{(10)}(0,\eta) + \hat{\boldsymbol{v}}^{(0)}(1,\eta). \tag{4.45}$$

Finally, the inhomogeneous boundary value problem for $\hat{\boldsymbol{v}}^{(2)}$ can only be solved if a solvability condition, similar to (4.30), is satisfied, and this condition would yield an expression for ω_1:

$$\omega_1 = \zeta k_1^2, \tag{4.46}$$

where ζ is a constant. Once this is determined, (4.39b) may be replaced by

$$\omega = \frac{1}{\epsilon}\left\{\omega_0 + \epsilon^2\zeta(k - \frac{\pi}{\epsilon})^2 + \cdots\right\}. \tag{4.47}$$

Making substitutions reversing those in (4.2) together with $k \to kL$, we obtain

$$\omega = \frac{v_o}{T}\left\{\omega_0 + \epsilon^2\zeta(\frac{kT}{\epsilon} - \frac{\pi}{\epsilon})^2 + \cdots\right\},$$

that is,

$$\omega_s = \omega_0 + \zeta(kT - \pi)^2 + \cdots. \tag{4.48}$$

This expression shows that the variation of ω_s around $kT = \pi$ has a quadratic behavior.

Our *Abaqus* simulations presented in the previous section have already computed ω_s for a discrete set of kT values in the reduced Brillouin zone, including when $kT = \pi$. Thus, ω_0 is already available. Although we could find ζ by implementing the above procedure on *Abaqus*, we decided to simply use the data set from the previous section, interpolate on *Mathematica* to obtain $\omega_s(kT)$, and finally obtain ζ using the formula $\zeta = \omega_s''(\pi)/2$. For the cases $\lambda_1 = 1, 0.8$, this procedure yields $\zeta = -2.624, -1.538$, respectively. The corresponding two-term asymptotic result (4.48) is displayed in Fig. 6 in black dashed lines near $kT = \pi$, and agrees well with the numerical results, as expected.

5. Surface wrinkling

Surface wrinkling can be studied by setting $\omega_s = 0$ in which case Eq. (3.24), namely $\det(\boldsymbol{M}) = 0$, becomes the bifurcation condition. It is found that for each set of material and geometrical parameters, the solution of this equation for λ_1 is independent of kT, similar to the case of a homogeneous half-space (the classical Biot problem) although kT does appear in the equation. For the typical case of $\alpha = 2$ and $\delta = 0.5$, solving this equation yields $\lambda_{1\mathrm{cr}} \approx 0.74037$, which has already been reported in Section 3. Fig. 7 displays the results for a selection of other values of α with δ fixed at 0.5, and confirms the fact that $\lambda_{1\mathrm{cr}}$ is independent of kT for each α.

To further understand the meaning of $\lambda_{1\mathrm{cr}}$ computed above, we first observe that for the periodic structure under consideration, there are three critical values of λ_1 (the Biot values): those associated with the orange material (denoted by $\lambda_{1cr}^{\mathrm{o}}$), the gray material (denoted by $\lambda_{1cr}^{\mathrm{g}}$), and the homogenized material (denoted by $\lambda_{1cr}^{\mathrm{h}}$), respectively. The dependence of these three critical stretches on α is displayed in Fig. 8. Note that whereas $\lambda_{1cr}^{\mathrm{g}}$ is a constant, $\lambda_{1cr}^{\mathrm{o}}$ is dependent on α. This is because the orange material is in a state of biaxial compression, which changes as α is varied.

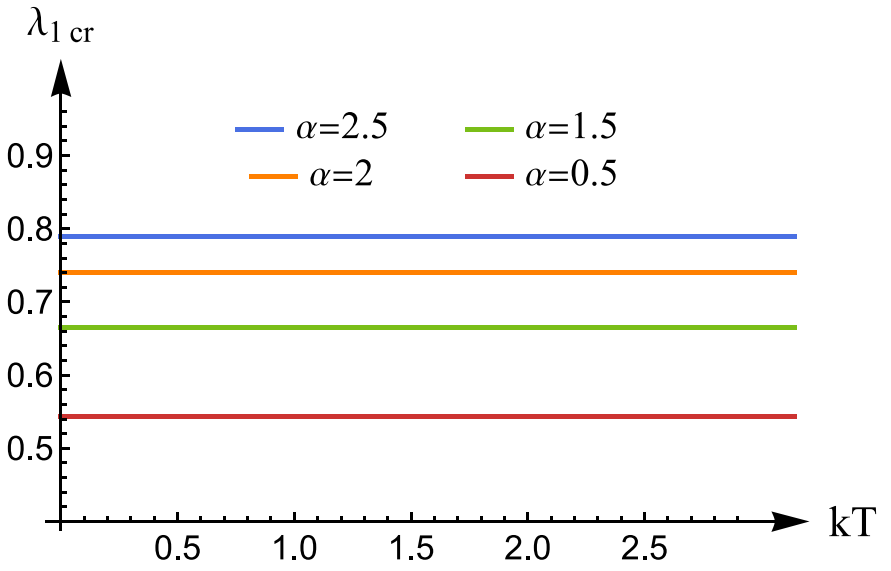


Fig. 7. Critical value of λ_1 of a periodic elastic half-space for four typical values of α when δ is fixed at 0.5.

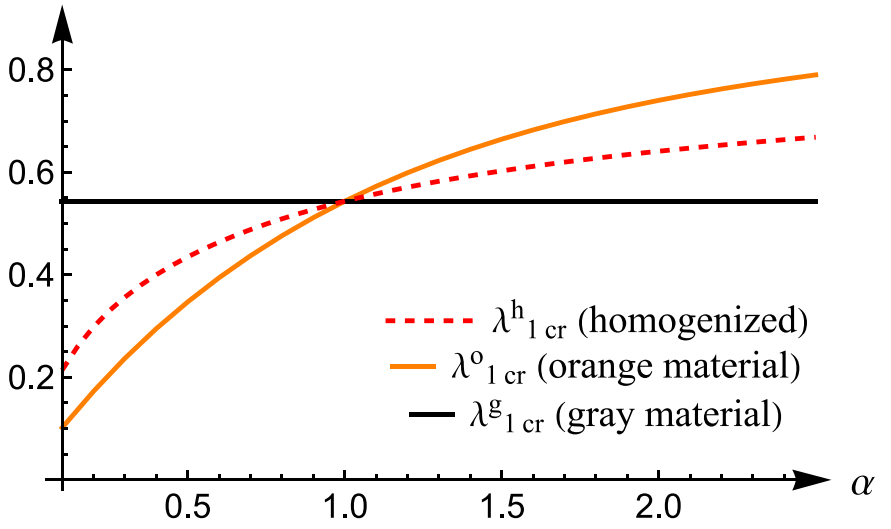


Fig. 8. Dependence on the modulus ratio α of the critical stretches associated with the homogenized (red dashed line), orange (orange line) and gray (black line) materials, respectively when $\delta = 0.5$. The critical stretch for the periodic half-space is always the maximum of these three critical stretches for each value of α.

It can be seen that $\lambda^{\mathrm{h}}_{1cr}$ always lies between $\lambda^{\mathrm{o}}_{1cr}$ and $\lambda^{\mathrm{g}}_{1cr}$ except at $\alpha = \mu_{\mathrm{g}}/\mu_{\mathrm{o}} = 1$ where the three values coincide. After we have computed λ_{1cr} and the associated λ^{g}_1 and λ^{o}_1 for each α, it is found that we always have $\lambda_{1cr} = \lambda^{\mathrm{g}}_1 = \lambda^{\mathrm{o}}_1$ up to two decimal places. This is not surprising since we have taken Poisson's ratio to be 0.4999 so that both materials can be viewed as incompressible, in which case continuity of λ_2 implies continuity of λ_1 across the interface. Furthermore, it is found that $\lambda_{1\mathrm{cr}} = \lambda^{\mathrm{g}}_{1cr}$ for $\alpha \le 1$ (gray material softer) and $\lambda_{1\mathrm{cr}} = \lambda^{\mathrm{o}}_{1cr}$ for $\alpha \ge 1$ (orange material softer). In other words,

$$\lambda_{1\mathrm{cr}} = \max\left\{\lambda^{\mathrm{o}}_{1cr}, \lambda^{\mathrm{g}}_{1cr}\right\}, \qquad 0 < \alpha < \infty, \tag{5.1}$$

and surface wrinkling is dictated by the softer of the two materials, or equivalently by the material more susceptible to surface wrinkling.

To verify whether the above conclusion is also applicable to compressible materials and other values of δ, we consider a typical case with $\nu = 1/4$, $\delta = 1/3$. When $\alpha = 0.5$, we find that

$$\lambda_{1\mathrm{cr}} = 0.6511, \qquad \lambda^{\mathrm{g}}_1 = \lambda^{\mathrm{g}}_{1cr} = 0.5266, \qquad \lambda^{\mathrm{o}}_1 = 0.7134, \qquad \lambda^{\mathrm{o}}_{1cr} = 0.5306, \tag{5.2}$$

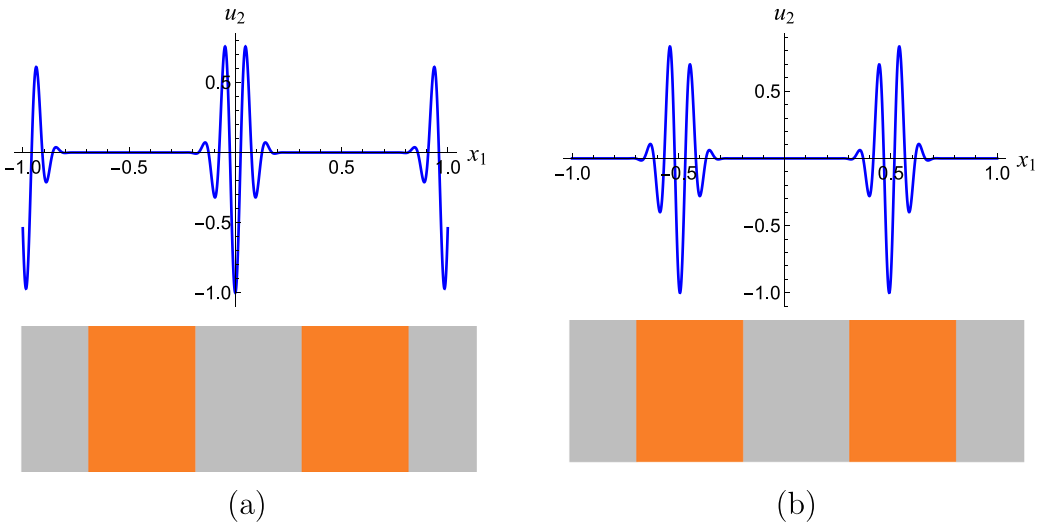


Fig. 9. The buckling modes of the periodic elastic half-space with $kT = 1$. (a) $\alpha = 0.5$ for which the gray material is more susceptible to surface wrinkling; (b) $\alpha = 2$ for which the orange material is more susceptible to surface wrinkling.

whereas when $\alpha = 2$, we obtain

$$\lambda_{1\mathrm{cr}} = 0.6074, \qquad \lambda_1^{\mathrm{g}} = 0.7308, \qquad \lambda_{1cr}^{\mathrm{g}} = 0.5266, \qquad \lambda_1^{\mathrm{o}} = \lambda_{1cr}^{\mathrm{o}} = 0.5457. \tag{5.3}$$

These two sets of results can be interpreted as follows. When $\alpha = 0.5$ (gray material is softer), the λ_1^{g} associated with the global Biot value $\lambda_{1\mathrm{cr}}$ is equal to the Biot value $\lambda_{1cr}^{\mathrm{g}}$ for the gray material and surface wrinkling is dictated by the gray material which is the material more susceptible to surface wrinkling. This is confirmed by the fact that when λ_1^{g} reaches $\lambda_{1cr}^{\mathrm{g}}$, λ_1^{o} (= 0.7134) has not yet reached $\lambda_{1cr}^{\mathrm{o}}$ (= 0.5306). In contrast, when $\alpha = 2$ (orange material is softer), the roles of the gray and orange materials are exchanged. In both cases, surface wrinkling is dictated by the material more susceptible to surface wrinkling as in the incompressible case. The only difference is that here $\lambda_{1\mathrm{cr}}$ is no longer equal to λ_1^{g} or λ_1^{o} because of compressibility and so the simple condition (5.1) no longer holds.

Having established (5.1) for incompressible materials, it is then of interest to investigate the profile of the displacement field and to check whether surface elevation would indeed be localized in the material more susceptible to surface wrinkling. The displacement field at the surface is computed with the aid of the truncated form of (3.15a), namely

$$\boldsymbol{u}(x_1, 0) = \sum_{n=-N}^{N} \boldsymbol{z}_n(0) \mathrm{e}^{\mathrm{i}k_n x_1} = \left(\mathrm{e}^{\mathrm{i}k_{-N}x_1}\boldsymbol{I}_{2\times 2}, \ldots, \mathrm{e}^{\mathrm{i}k_0 x_1}\boldsymbol{I}_{2\times 2}, \ldots, \mathrm{e}^{\mathrm{i}k_N x_1}\boldsymbol{I}_{2\times 2}\right)\boldsymbol{z}(0), \tag{5.4}$$

where $\boldsymbol{z}(0)$ is the non-trivial solution of $\boldsymbol{M}\boldsymbol{z}(0) = \boldsymbol{0}$. Both the real and imaginary parts of the right hand side are eigensolutions.

Fig. 9 shows the real part of $u_2(x_1, 0)$ (vertical surface displacement) of the bifurcation mode for two representative cases: $\alpha = 0.5$ and $\alpha = 2$. When $\alpha = 0.5$, the gray material is softer, and the displacement is primarily concentrated in the gray material region, while the surface displacement of the orange material is negligible. Conversely, when $\alpha = 2$, the orange material is softer, and the displacement is predominantly localized in the orange material region, with the surface displacement of the gray material being nearly zero. Thus, these additional results serve to confirm the earlier claim that surface wrinkling is dictated by the softer material and also the fact that Biot instability exhibits no preferred wavelength and so it can be accommodated over any finite segment.

This complete localization – the fact that the stronger material shows essentially no deformation at all rather than merely less deformation – can be understood from the structure of the bifurcation condition (5.1) itself. The composite structure reaches criticality precisely when the *local* stretch state of the weaker material coincides with the Biot point of that same material considered in isolation; at this same value of λ_1, the stronger material's own surface impedance matrix remains strictly positive definite. The weaker material's marginal condition is therefore entirely self-sufficient: it does not require any cooperative deformation of its neighbor to become satisfied. Moreover, since this local bifurcation condition is independent of wavenumber, it inherits the same ill-posedness with respect to spatial pattern selection that underlies localized creasing in the classical (homogeneous) Biot problem (Gent & Cho, 1999; Hong et al., 2009; Ogden & Fu, 1996): there is no distinguished lengthscale, and the bifurcation mode is free to organize itself, through superposition of the Fourier harmonics in (3.15a), into a profile that has already effectively decayed to zero by the time it reaches the material interfaces. Complete localization in the weaker material is not simply a consequence of one material being "softer" than the other in some relative sense; it reflects the fact that, at the critical stretch, only the weaker material's local elasticity supports a genuinely marginal (zero-cost) deformation mode, while the stronger material remains incapable of sustaining one.

6. Summary

In this paper, we have analytically examined the effect of prestress on the propagation of surface waves in a periodic hyperelastic half-space. Our approach combines Floquet-Bloch theory, Fourier series expansion, and the Stroh formalism. In contrast to the eigensolution-based methods used in most previous studies, this framework avoids expressing the solution as a linear combination of eigenmodes associated with the governing equations. The eigensolutions approach typically produces spurious modes that must be identified and eliminated through careful tracking of all the eigenvalues, a task that becomes increasingly burdensome as the truncation number grows and the dimensionality of the problem escalates. By contrast, the surface impedance method based on the Stroh formalism offers a more robust and efficient alternative, as it circumvents the direct computation of eigenvalues and eigenvectors of high-dimensional matrices. Moreover, within the subsonic regime, the surface impedance matrix is Hermitian, ensuring that all its eigenvalues are real. As a result, the condition for the existence of surface waves, namely the vanishing of the determinant of the impedance matrix, can be equivalently expressed as the requirement that its minimum eigenvalue approaches zero. This reformulation avoids the numerical instability associated with determinant evaluation for large matrices and significantly enhances computational efficiency.

We found that as the pre-stretch is decreased, the surface wave speed decreases but remains a function of the wavenumber. However, as the pre-stretch reaches a critical value, the wave speed becomes zero for all wavenumbers and surface wrinkling is localized in the material that is more susceptible to surface wrinkling. This may not be so surprising in view of the fact that the Biot instability is known to be independent of wavenumbers and it can adjust its wavelength to fit any finite domain. What is perhaps surprising is the fact that our truncation scheme is capable of predicting this phenomenon. Although homogenized material properties were also derived, our analysis demonstrates that surface wrinkling is not governed by these effective properties. In this respect, our findings echo the distinction between microscopic and macroscopic instabilities identified by Triantafyllidis and Maker (1985) in two-phase composites. While homogenization provides a convenient theoretical framework, over-reliance on it may obscure the onset of localized (microscopic) instabilities that precede global (macroscopic) failure, potentially leading to inaccurate predictions of structural stability.

For analytical tractability, we have assumed a piecewise uniform prestress distribution, which is generally compatible only with piecewise homogeneous materials. In more general periodic media, prestress is expected to vary spatially, and the analysis of wave propagation and surface instability would necessarily rely on fully numerical approaches. It is anticipated that the present semi-analytical results will serve as useful benchmark solutions for such future investigations.

CRediT authorship contribution statement

Yuxin Fu: Writing – review & editing, Writing – original draft, Visualization, Validation, Software, Methodology, Investigation, Formal analysis. **Michel Destrade:** Writing – review & editing, Visualization, Supervision, Resources, Project administration, Investigation. **Yuesheng Wang:** Writing – review & editing, Supervision, Resources, Project administration, Funding acquisition, Conceptualization. **Yibin Fu:** Writing – review & editing, Writing – original draft, Visualization, Validation, Supervision, Software, Resources, Project administration, Methodology, Investigation, Funding acquisition, Formal analysis, Conceptualization.

Declaration of competing interest

The authors declare that they have no known competing financial interests or personal relationships that could have appeared to influence the work reported in this paper.

Acknowledgments

This work was supported by the National Natural Science Foundation of China (Grant No 12472067) and the Engineering and Physical Sciences Research Council, UK (Grant No EP/W007150/1). Part of this research was carried out when the first author was visiting the University of Galway supported by a grant from the China Scholarship Council.

Data availability

Data will be made available on request.

References

Aberg, M., & Gudmundson, P. (1997). The usage of standard finite element codes for computation of dispersion relations in materials with periodic microstructure. *Journal of the Acoustical Society of America*, *102*, 2007–2013.

Assouar, M. B., & Oudich, M. (2011). Dispersion curves of surface acoustic waves in a two-dimensional phononic crystal. *Applied Physics Letters*, *99*, Article 123505.

Bakhvalov, N., & Panasenko, G. (1989). *Homogenization: averaging processes in periodic media*. Dordrecht, MA: Kluwer.

Barnett, D. M., & Lothe, J. (1974). Consideration of the existence of surface wave (rayleigh wave) solutions in anisotropic elastic crystals. *Journal of Physics F*, *4*, 671–686.

Barnett, D. M., & Lothe, J. (1985). Free surface (rayleigh) waves in anisotropic elastic half-spaces: the surface impedance method. *Proceedings of the Royal Society A*, *402*, 135–152.

Bensoussan, A., Lions, J., & Papanicolaou, G. (1978). *Asymptotic analysis for periodic structures*. The Netherlands: North-Holland.

Biot, M. A. (1963). Surface instability of rubber in compression. *Applied Scientific Research A*, *12*, 168–182.

Biryukov, S. (1985). Impedance method in the theory of elastic surface waves. *Soviet Physics. Acoustics*, *31*, 350–354.

Bowden, N., Brittain, S., Evans, A. G., Hutchinson, J. W., & Whitesides, G. M. (1998). Spontaneous formation of ordered structures in thin films of metals supported on an elastomeric polymer. *Nature*, *393*, 146–149.

Cai, Z. X., & Fu, Y. B. (1999). On the imperfection sensitivity of a coated elastic half-space. *Proceedings of the Royal Society A*, *455*, 3285–3309.

Chadwick, P. (1997). The application of the stroh formalism to prestressed elastic media. *Mathematics and Mechanics of Solids*, *2*, 379–403.

Chadwick, P., & Ogden, R. W. (1971). On the definition of elastic moduli. *Archive for Rational Mechanics and Analysis*, *44*, 41–53.

Chadwick, P., & Smith, G. D. (1977). Foundations of the theory of surface waves in anisotropic elastic materials. *Advances in Applied Mechanics*, *17*, 303–376.

Craster, R. V., Kaplunov, J., Nolde, E., & Guenneau, S. (2012). Bloch dispersion and high frequency homogenization for separable doubly-periodic structures. *Wave Motion*, *49*, 333–346.

Craster, R. V., Kaplunov, J., & Pichugin, A. V. (2010). High-frequency homogenization for periodic media. *Proceedings of the Royal Society A*, *466*, 2341–2362.

Darinskii, A. N., & Shuvalov, A. L. (2020). Surface electromagnetic waves in anisotropic superlattices. *Physical Review A*, *102*, Article 033515.

Destrade, M., & Ogden, R. W. (2005). Surface waves in a stretched and sheared incompressible elastic material. *International Journal of Non-Linear Mechanics*, *40*, 241–253.

Dimmock, R. L., Wang, X. L., Fu, Y., El Haj, A. J., & Yang, Y. (2020). Biomedical applications of wrinkling polymers. *Recent Progress in Materials*, *2*, Article 2001005.

Djafari-Rouhani, B., Maradudin, A. A., & Wallis, R. F. (1984). Rayleigh waves on a superlattice stratified normal to the surface. *Physical Review B*, *29*, 6454–6462.

Dowaikh, M. A., & Ogden, R. W. (1990). On surface waves and deformations in a pre-stressed incompressible elastic solid. *IMA Journal of Applied Mathematics*, *44*, 261–284.

Flavin, J. (1963). Surface waves in pre-stressed mooney material. *The Quarterly Journal of Mechanics and Applied Mathematics*, *16*, 441–449.

Fu, Y. B. (2005a). An explicit expression for the surface-impedance matrix of a generally anisotropic incompressible elastic material in a state of plane strain. *International Journal of Non-Linear Mechanics*, *40*, 229–239.

Fu, Y. B. (2005b). An integral representation of the surface-impedance tensor for incompressible elastic materials. *Journal of Elasticity*, *81*, 75–90.

Fu, Y. B., & Mielke, A. (2002). A new identity for the surface–impedance matrix and its application to the determination of surface-wave speeds. *Proceedings of the Royal Society A*, *458*, 2523–2543.

Gent, A. N., & Cho, I. S. (1999). Surface instabilities in compressed or bent rubber blocks. *Rubber Chemistry & Technology*, *72*, 253–262.

Genzer, J., & Groenewold, J. (2006). Soft matter with hard skin: from skin wrinkles to templating and material characterization. *Soft Matter*, *2*, 310–323.

Green, A. E., & Zerna, W. (1954). *Theoretical Elasticity*. Oxford: Oxford University Press.

Hong, W., Zhao, X., & Suo, Z. (2009). Formation of creases on the surfaces of elastomers and gels. *Applied Physics Letters*, *95*, Article 111901.

Hu, L. X., Liu, L. P., & Bhattacharya, K. (2012). Existence of surface waves and band gaps in periodic heterogeneous half-spaces. *Journal of Elasticity*, *107*, 65–79.

Khelif, Z., Achaoui, Y., Benchabane, S., Laude, V., & Aoubiza, B. (2010). Locally resonant surface acoustic wave band gaps in a two-dimensional phononic crystal of pillars on a surface. *Physical Review B*, *81*, Article 214303.

Laude, V., Wilm, M., Benchabane, S., & Khelif, A. (2005). Full band gap for surface acoustic wave in a piezoelectric phononic crystal. *Physical Review E*, *71*, Article 036607.

Li, B., Cao, Y. P., Feng, X. Q., & Gao, H. J. (2012). Mechanics of morphological instabilities and surface wrinkling in soft materials: a review. *Soft Matter*, *8*, 5728–5745.

Li, G. Y., Xu, G. Q., Zheng, Y., & Cao, Y. P. (2018). Non-leaky modes and bandgaps of surface acoustic waves in wrinkled stiff-film/compliant-substrate bilayers. *Journal of the Mechanics and Physics of Solids*, *112*, 239–252.

Li, G. Y., Zheng, Y., Cao, Y. P., Feng, X. Q., & Zhang, W. Y. (2016). Controlling elastic wave propagation in a soft bilayer system via wrinkling-induced stress patterns. *Soft Matter*, *12*, 4204.

Manzanares-Martinez, B., & Ramos-Mendieta, F. (2003). Surface elastic waves in solid composites of two-dimensional periodicity. *Physical Review B*, *68*, Article 134303.

Matysiak, S. J., Mieszkowski, R., & Perkowski, D. M. (2009). Surface waves in a periodic two-layered elastic half-space with the boundary normal to the layering. *Acta Mechanica*, *207*, 235–243.

Mielke, A., & Fu, Y. B. (2004). Uniqueness of the surface-wave speed: a proof that is independent of the stroh formalism. *Mathematics and Mechanics of Solids*, *9*, 5–15.

Newell, A. C. (1974). *Nonlinear wave motion (AMS lectures in appl. math. 15)*. AMS, New York.

Norris, A. N., Shuvalov, A. L., & Kutsenko, A. A. (2013). The matrix sign function for solving surface wave problems in homogeneous and laterally periodic elastic half-spaces. *Wave Motion*, *50*, 1239–1250.

Ogden, R. W., & Fu, Y. B. (1996). Post-buckling of a pre-stressed elastic halfspace. In *Contemporary research in the mechanics and mathematics of materials (Eds R C Batra and M F Beatty)* (pp. 164–175). Barcelona.

Pu, X. B., & Shi, Z. F. (2017). A novel method for identifying surface waves in periodic structures. *Soil Dynamics and Earthquake Engineering*, *98*, 67–71.

Rudykh, S., & Boyce, M. C. (2014). Transforming wave propagation in layered media via instabilities-induced interfacial wrinkling. *Physical Review Letters*, *112*, Article 034301.

Shuvalov, A. L. (2009). Existence and spectral properties of shear horizontal surface acoustic waves in vertically periodic half-spaces. *Proceedings of the Royal Society A*, *465*, 1489–1511.

Shuvalov, A. L. (2024). The stroh formalism for acoustic waves in 1d-inhomogeneous media: unified background and some applications. ArXiv. 2412.09138.

Stroh, A. N. (1958). Dislocations and cracks in anisotropic elasticity. *Philosophical Magazine*, *3*, 625–646.

Stroh, A. N. (1962). Steady state problems in anisotropic elasticity. *Journal of Mathematical Physics*, *41*, 77–103.

Tanaka, Y., & Tamura, S. I. (1998). Surface acoustic waves in two-dimensional periodic elastic structures. *Physical Review B*, *58*, 7958–7965.

Tanaka, Y., & Tamura, S. I. (1999). Acoustic stop bands of surface and bulk modes in two-dimensional phononic lattices consisting of aluminium and a polymer. *Physical Review B*, *60*, 13294–13297.

Tanaka, Y., Yano, T., & Tamura, S. (2007). Surface guided waves in two-dimensional phononic crystals. *Wave Motion*, *44*, 501–512.
Ting, T. C. T. (1996). *Anisotropic elasticity: Theory and applications*. Oxford: Oxford University Press.
Triantafyllidis, N., & Maker, B. (1985). On the comparison between microscopic and macroscopic instability mechanisms in a class of fiber-reinforced composites. *Transactions of the ASME. Journal of Applied Mechanics*, *52*, 794–800.
Wang, L. F., & Bertoldi, K. (2012). Mechanically tunable phononic band gaps in three-dimensional periodic elastomeric structures. *International Journal of Solids and Structures*, *49*, 2881–2885.
Wu, T. T., Hsu, Z. C., & Huang, Z. G. (2005). Band gaps and electromechanical coupling coefficient of a surface acoustic wave in a two-dimensional piezoelectric phononic crystal. *Physical Review B*, *71*, Article 064303.
Wu, T. T., Huang, Z. G., & Lin, S. (2004). Surface and bulk acoustic waves in two-dimensional phononic crystal consisting of materials with general anisotropy. *Physical Review B*, *69*, Article 094301.
Yan, Z. Z., & Wang, Y. S. (2008). Calculation of band structures for surface waves in two-dimensional phononic crystals with a wavelet-based method. *Physical Review B*, *78*, Article 094306.
Yang, S., Khare, K., & Lin, P. C. (2010). Harnessing surface wrinkle patterns in soft matter. *Advanced Functional Materials*, *20*, 2550–2564.